ACS OMEGA

Article

Cite This: ACS Omega 2018, 3, 1244−1262

Mechanistic Insight into Size-Dependent Enhanced Cytotoxicity of Industrial Antibacterial Titanium Oxide Nanoparticles on Colon Cells Because of Reactive Oxygen Species Quenching and Neutral Lipid Alteration

Suresh K. Verma,[†] Ealisha Jha,[‡] Pritam Kumar Panda,[†] Arun Thirumurugan,[§] S. K. S. Parashar,[∥] Shubhransu Patro,[⊥] and Mrutyunjay Suar*[,†]

[†]School of Biotechnology, [∥]School of Applied Sciences, and [⊥]Kalinga School of Medical Sciences, KIIT University, Bhubaneswar, Orissa 751024, India

[‡]Department of Physics and Physical Oceanography, Memorial University of Newfoundland, St. John's, Newfoundland and Labrador NL A1C 5S7, Canada

[§]Advanced Materials Laboratory, Department of Mechanical Engineering, Faculty of Mathematical and Physical Sciences, University of Chile, Av. Beauchef 851, piso 5, Santiago, Chile

Supporting Information

ABSTRACT: This study evaluates the impact of industrially prepared TiO_2 nanoparticles on the biological system by using an in vitro model of colon cancer cell lines (HCT116). Industrial synthesis of titanium oxide nanoparticles was mimicked on the lab scale by the high-energy ball milling method by milling bulk titanium oxide particles for 5, 10, and 15 h in an ambient environment. The physiochemical characterization by field emission scanning electron microscopy, dynamic light scattering, and UV−visible spectroscopy revealed alteration in the size and surface charge with respect to increase in the milling time. The size was found to be reduced to 82 ± 14, 66 ± 12, and 42 ± 10 nm in 5, 10, and 15 h milled nano TiO_2 from 105 ± 12 nm of bulk TiO_2, whereas the zeta potential increased along with the milling time in all biological media. Cytotoxicity and genotoxicity assays performed with HCT116 cell lines by MTT assay, oxidative stress, intracellular lipid analysis, apoptosis, and cell cycle estimation depicted cytotoxicity as a consequence of reactive oxygen species quenching and lipid accumulation, inducing significant apoptosis and genotoxic cytotoxicity. In silico analysis depicted the role of Sod1, Sod2, p53, and VLDR proteins−TiO_2 hydrogen bond interaction having a key role in determining the cytotoxicity. The particles exhibited significant antibacterial activities against *Escherichia coli* and *Salmonella typhimurium*.

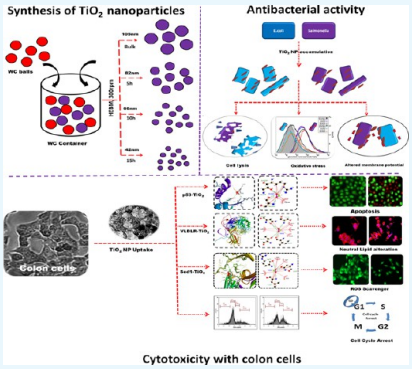

1. INTRODUCTION

Titanium oxide nanoparticles and their bulk counterpart have gained a lot of attention in research and industry in the last few decades. They have been widely engineered and used in sunscreen and cosmetics because of their absorptive properties.[1] A lot of food products such as candies, sweets, and chewing gums use TiO_2 as one of its contents. Other TiO_2 applications include antimicrobial application, medical application, and energy storage.[2] TiO_2 with food-grade pigment has been used as a whitening agent in many foods and drugs[3] and as a digestion marker.[4] Many food safety agencies such as the Food and Drug Administration and the European Food Safety Authority (EFSA) have approved TiO_2 and its nanocrystalline form as a food additive and for drug dosage up to a level.[3] Moreover, it has been listed in the EU Annex II of Regulation 1333/2008 as a permitted color additive in foods at Good Manufacturing Practices levels.

With the increase in demand for TiO_2 and its nanoparticles, their production has increased in large quantities, with different properties according to the need. The production is expected to increase exponentially in the coming decade. Researchers and industries are using a variety of methods to synthesize them. Some of the common procedures include synthesis by using hydrolysis of titanium salts (Ti) acidic solution.[5] Controlled synthesis in respect of shape, size, and structure has been carried out by using chemical vapor condensation or nucleation from sol−gel.[6] Though these methods are successful in synthesizing TiO_2 nanoparticles, there is a limitation of bulk production. It also raises a question about the purity because of the use of different chemicals. Physical methods such as high-energy ball milling (HEBM) have been proved as a potential

Received: October 9, 2017
Accepted: January 15, 2018
Published: January 30, 2018

DOI: 10.1021/acsomega.7b01522
ACS Omega 2018, 3, 1244−1262

solution for this problem. Indris et al. and many other groups have successfully reported the synthesis of the impurity-free and pure form of TiO_2 by the high-energy milling method.[7] These mechanically synthesized TiO_2 nanoparticles have been explored for their worldwide physical as well as chemical applications. TiO_2 nanoparticles have also been recognized for use in many biological applications owing to their antibacterial properties.[8] Though the biological application and effects of TiO_2 nanoparticles prepared by other methods have been studied a lot, there is no report on the effect of industrially prepared and commonly used mechanically milled TiO_2 nanoparticles till date. Previous literature has defined the biological activities of TiO_2 nanoparticles and tested them, but has reported that the nanoparticles have been synthesized on the lab scale.[8] The reported results are debatable while considering the effects of TiO_2 nanoparticles in the real world because most of the used TiO_2 nanoparticles are prepared on the industrial scale. Keeping in view the importance of the demands and potential of preparation of TiO_2 nanoparticles on the industrial scale by the high-energy milling process, it is essential to understand the effect of these particles on a biological system. This study investigates and reports this aspect of TiO_2 nanoparticle effects on the biological system.

Preparation and consumption of TiO_2 nanoparticles have been a matter of concern over their effect on human society. The nanoparticles can interact with human body through three basic entry points: (a) skin cells directly, (b) lung cells through inhalation, and (c) digestive tract epithelial cells after oral ingestion. However, lung cell interaction and digestive tract interaction are the major concerns. Recent reports have mentioned the regular oral intake of TiO_2 nanoparticles inside the human body as an additive with food products and toothpaste.[9] With increasing concern over the extensive use of these nanoparticles in food additives and drugs nowadays, their cytotoxic effect requires extensive study. Several studies over the last decades have reported the in vitro and in vivo toxicological effect of TiO_2 nanoparticles on different cell lines and live models. TiO_2 nanoparticles prepared by chemical methods have been checked for their cytotoxic behavior with various cell models such as fibroblasts, macrophages, keratinocytes, epithelial cells, and liver cells.[10] Previous studies have reported the nature and mechanism of cytotoxicity of TiO_2 nanoparticles with human lung cancer cell lines.[11] Thevenot et al.[12] and Krüger group[13] have recently demonstrated the mechanism of cytotoxicity effect on different colon cancer cell lines. Many colon carcinogenic cell lines such as Ls174-t and HT-29 have been used for understanding the cytotoxic effect of nanoparticles on colon cells.[12,13] Human colon carcinogenic cell line HCT116 has been recognized as one of the most important types of colon cancer cell lines for different molecular as well as cancer studies because of its wild-type specificity.[14] However, the knowledge regarding the cytotoxic effect of TiO_2 nanoparticles on this cell line is still lacking. This article addresses this issue by reporting the cytotoxic effect and the probable mechanism of TiO_2 nanoparticle interaction with HCT116 colon carcinogenic cell lines.

A limited number of pathological outcomes are integrated from multiple pathways of toxicity by biological systems including apoptosis, inflammation, fibrosis, hypertrophy, metaplasia, and carcinogenesis.[15] Till date, the various factors that have been reported to determine the cytotoxic effect of nanoparticles are (1) internalization of nanoparticles into cells,[16] (2) production of reactive oxygen species (ROS),[17] and (3) DNA damage.[18] Effect of TiO_2 nanoparticles as a function of ROS production and cell damage has been well-reported by Gurr et al.[19] and Long group[20] on human bronchial epithelial cells and brain microglia. A number of groups have also reported the size and shape of the nanoparticle as an important factor for their cytotoxic effects on cell lines.[21] In addition to this, the charge of the nanoparticles has also been found to play an important role in deciding the extent of cytotoxicity of nanoparticles.[22] These studies emphasized the effect of particle charge and zeta potential on the surface of the cell, whereas their effect on the surface charge of cells is still undiscovered. Oxidative stress and genotypic alteration have been reported as a mechanism of cytotoxicity of TiO_2 nanoparticles,[23] however, the effect on lipid production in cells on interaction with the nanoparticles is still to be understood. This article investigates and reports these cytotoxic effects in relation with TiO_2 nanoparticles, synthesized by the HEBM technique as an industrial prototype. The surface charge of cells was reported to be significantly changed with a reasonable change in the lipid metabolism and apoptosis inside colon cells treated by TiO_2 nanoparticles. Moreover, the most interesting finding was the ROS quenching by TiO_2 nanoparticles playing an important role in the mechanism of cytotoxicity and the in silico investigation, which revealed the interaction of TiO_2 nanoparticles with Sod1, tp53, and VLDLR amino acid residues as a probable cause of cellular metabolism processes.

In addition to this, the antibacterial effect of TiO_2 nanoparticles has been a matter of long discussion for decades.[8] We have also determined the antibacterial effect of industrially synthesized TiO_2 nanoparticles with bacterial strains *Escherichia coli* and *Salmonella typhimurium*. A significant difference in bacteria death was found after treatment with TiO_2 nanoparticles. The effect of the surface charge of nanoparticles has been reported as an important factor in the antibacterial properties of the nanoparticles.[24,25] The mechanism of ROS production in bacteria exposed to nanoparticles has been a well-discovered phenomenon.[26] This report enlightens the effect of TiO_2 nanoparticle interaction on the surface charge of bacteria as well as their consequences on the ROS production.

2. MATERIALS AND METHODS

2.1. Chemicals and Instruments. TiO_2 powder was purchased from Merck. Milling was performed in a horizontal oscillatory mill (Retsch, PM400) operating at 25 Hz. Particles were sonicated using a probe sonicator (Vibra-Cell, VCX130, Sonics, USA) in Milli-Q water medium. TiO_2 dispersions were characterized by the hydrodynamic diameter and zeta potential by dynamic light scattering (DLS) using a Zetasizer Nano system (Malvern Instruments, UK). 3-(4,5-Dimethyl-thiazol-2-yl)-2,5-diphenyl tetrazolium bromide (MTT) cell culture reagent was purchased from Himedia (India). 2,7-Dichlorofluorescein diacetate (H_2DCFDA) was purchased from Sigma-Aldrich. LipidTOX Deep Red neutral, Alexa Fluor, phalloidin, Hoechst, and Syto 9 were purchased from Invitrogen (Carlsbad, CA). Flow cytometry experiments were performed on an Attune acoustic focusing cytometer (Thermo Scientific, USA).

2.2. Synthesis of TiO_2 Nanoparticles. TiO_2 nanoparticles were synthesized by the HEBM method by milling titanium oxide powder (Merck) in tungsten carbide cells (250 mL) using hardened tungsten carbide (10 mm) balls at 300 rpm in an

DOI: 10.1021/acsomega.7b01522
ACS Omega 2018, 3, 1244−1262

ambient atmosphere for 5, 10, and 15 h. The mechanical milling was performed in a horizontal oscillatory mill (Retsch, PM400) operating at 25 Hz. The mixture ratio of tungsten balls and TiO_2 powders was 10:1 by weight percent.

2.3. Physiochemical Characterization of Bulk and Nano TiO_2. The synthesized TiO_2 nanoparticles were characterized for size, size distribution, and charge. Nanoparticle suspensions were prepared by suspending TiO_2 nanoparticles, synthesized by milling at different time durations, in Milli-Q water, phosphate-buffered saline (PBS), and Dulbecco's modified Eagle medium (DMEM) cell culture complete medium and sonicating for 15 min at 50 amplitude and 100 W. Measurement of size was carried out by a Zetasizer Nano system (Malvern Instruments) by DLS techniques. Zeta potential was also measured by the Zetasizer with the different medium suspensions of TiO_2 nanoparticles. Ultraviolet−visible (UV−vis) spectrum was obtained by taking the spectrum of the suspension in a range of 200−800 nm in UV−vis near-infrared spectrophotometer (Cary 60, Agilent).

2.4. Cell Culture and TiO_2 Nanoparticles Treatment. All nanoparticle solutions used for experimentation were freshly prepared and sonicated before treatment. Nanoparticles were sterilized with UV exposure prior to the treatment. HCT116 (colon cancer cell lines) were procured from NCCS Pune, India. Cells were cultured in DMEM (PAN Biotech) consisting of 10% fetal bovine serum (Himedia), 100 U/mL penicillin, 100 μg/mL streptomycin, and 2 mM L-glutamine (complete medium). Cells were maintained in a 25 cm^2 flask and were passaged at 70−80% confluency every 2−4 days.

2.5. Bacterial Culture and Strains. For each microbiological experiment, all glassware were sterilized by autoclaving at 120 °C for 15 min. The culture of *S. typhimurium* SL4522 and *E. coli* ATCC25922 strains were grown on lysogeny broth (LB) media by incubating overnight at 150 rpm and 37 °C and then subcultured for 4 h in 5 mL of LB media. They were harvested for experiments when the optical density (OD_{600}) reached 0.4 (logarithmic phase) by centrifuging and washing with PBS to have a final bacterial concentration of approximately ~10^6 to 10^7 cfu/mL.

2.6. Zeta Potential Measurement of HCT116 Cell Lines. The surface charge corresponding to the zeta potential of HCT116 cell lines was determined by the Zetasizer Nano system in DMEM complete medium. Prior to coincubation, the cells were seeded in a 24-well plate at a cell density of 1×10^5 cells/well in DMEM complete medium for 24 h. Different TiO_2 nanoparticles with a concentration of 50 and 250 μg/mL were coincubated with seeded cells after 24 h and incubated for next 24 and 48 h in a fully humidified atmosphere at 37 °C with 5% CO_2. Following incubation, the zeta potential was measured in a dip cell cuvette (Malvern Instruments) after gentle scraping of cells and washing with DMEM complete media to remove the debris.

2.7. Surface Charge Analysis of Bacterial Strains. Effect on the surface charge of the bacterial membrane after treatment with TiO_2 bulk and TiO_2 nanoparticles was analyzed by the Zetasizer (Malvern) in PBS medium. A simple methodology was followed as the harvested bacterial culture with 0.4 OD_{600} was treated with TiO_2 bulk and TiO_2 nanoparticles with different concentrations for 4 h at 37 °C. Followed by incubation, they were washed with PBS and analyzed for their zeta potential.

2.8. MTT Assay for Cell Viability. HCT116 cell viability was determined by the MTT assay, which is a colorimetric assay depicted by measuring the intensity of the purple color of the buffer (11 g of sodium dodecyl sulfate in 50 mL of 0.02 M HCl and 50 mL of isopropanol), which dissolves the formazan crystals produced by the reduction of MTT. The absorbance was taken at 570 nm in an ELISA plate reader (Epoch, BioTek, Germany). The amount of color product formed was proportional to the number of viable cells. Mean absorbance of nontreated cells was taken as a reference value for calculating 100% cellular survivability.

2.9. Flow Cytometry Analysis. *2.9.1. Cellular Uptake of Nanoparticles in Cell Lines.* Cellular uptake of nanoparticles was determined by flow cytometry using the method described by Zucker et al.[27] In brief, HCT116 cells were seeded in a 24-well plate at a cell density of 1×10^5 cells/well and incubated for 24 h. After incubation, 50 and 250 μg/mL of TiO_2 nanoparticles (bulk, 5, 10, and 15 h) were coincubated for 24 and 48 h. Following coincubation, the cells were trypsinized, centrifuged at 135*g* for 10 min, resuspended in 500 μL of medium, and kept on ice. Internalization was accessed in three independent experiments. The data were processed in FCS Express 5 (Denovo, Los Angeles, CA).

The flow cytometer used was Attune acoustic focusing cytometer (Applied Biosystems, Life technologies) equipped with a 488 nm argon laser. The cytometer was set up to measure forward scatter (FSC) linearly and side scatter (SSC) logarithmically. The nanoparticles (1 mg/mL) were run first to set the maximum SSC and minimum FSC signals.

2.9.2. Analysis of ROS Production in Cell Lines and Bacterial Strain. The ROS was qualitatively and quantitatively analyzed by the detection of the green signal of 2′,7′-dichlorodihydrofluorescein (DCF) in a BL1 filter (530/30) of the flow cytometer. The green signal corresponds to the number of DCF molecules produced by oxidation of the DCFDA dye by the ROS produced by cells (Kumar et al. 2011). Forward and side-scatter dot plots were used to gate out cellular fragments. For cell lines, trypsinized cells after treatment were washed with PBS and stained with DCFDA. For the bacterial cell analysis, the cells were washed with cold PBS after treatment for 4 h and then resuspended in cold PBS (pH 7.4). The suspension was then stained by DCFDA for flow cytometry analysis.

2.9.3. Analysis of Lipid Metabolism in Cell Lines. Intracellular accumulations of lipid droplets (LDs) triggered by the TiO_2 nanoparticles were analyzed with LipidTOX Deep Red neutral stain (H34477) in the BL2 filter (574/26) of the flow cytometer. The dye binds to the triggered neutral LDs accumulated intracellularly by the action of TiO_2 nanoparticles on HCT116 cells.

2.9.4. Cell Cycle Analysis in Cell Lines. For the cell cycle analysis of HCT116 cell lines, the cells were treated with different types of TiO_2 nanoparticles for 24 and 48 h after overnight incubation of the seeded cells with a density of 1×10^5 cells/well in a 24-well plate. Following this, trypsinization was done, and the cells were kept in ice. For the flow cytometry analysis, the cells were incubated with 1:2 dilution in 0.5% NP-40 nonionic detergent made up with PBS without Ca^{2+} and Mg^{2+}. Then, staining was done with propidium iodide (PI, 20 μg/mL, MP Biomedical, USA). Nuclei measurement was performed by the BL3 filter (640LP) of the flow cytometer. Nuclei subpopulations were analyzed by FCS Express 5 analysis software (De novo, Los Angeles, CA), and the cells with different phases were calculated from the histogram using the

DOI: 10.1021/acsomega.7b01522
ACS Omega 2018, 3, 1244−1262

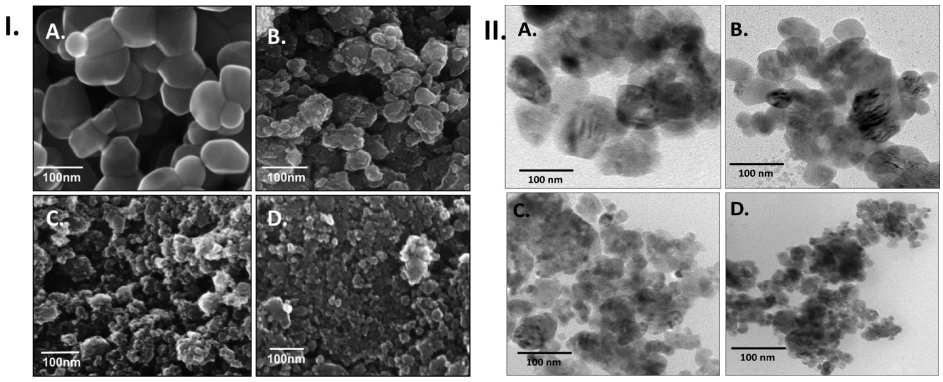

Figure 1. Characterization of TiO_2 nanoparticles prepared by the HEBM method. FESEM and transmission electron microscopy image of TiO_2 nanoparticles prepared by the HEBM method. (A) Bulk TiO_2, (B) 5 h nano TiO_2, (C) 10 h nano TiO_2, and (D) 15 h nano TiO_2. The scale bar denotes 100 nm.

Table 1. Physiochemical Characterization of Titanium Oxide Nanoparticles; Table Shows the Size Determined by FESEM and the Hydrodynamic Diameter and Zeta Potential of TiO_2 Nanoparticles in Different Media[a]

		hydrodynamic diameter (nm)			zeta potential (mV)			
nanoparticles	size (nm) by FESEM	aq	PBS	DMEM (complete)	aq	PBS	DMEM (complete)	band gap (eV)
bulk TiO_2 particles	100 ± 10	268.2 ± 68	269.3 ± 20	435.9 ± 36	−46.6 ± 7.7	−67.6 ± 4.3	−32.9 ± 2.3	3.4
5 h nano TiO_2 particles	80 ± 10	239.2 ± 29	199.9 ± 12	321.8 ± 24	−38.2 ± 7.1	−56.4 ± 5.7	−28.2 ± 1.5	3.8
10 h nano TiO_2 particles	60 ± 10	185.5 ± 28	167.8 ± 30	256.8 ± 14	−26.4 ± 6.8	−45.4 ± 3.9	−18.6 ± 5.7	4.2
15 h nano TiO_2 particles	40 ± 10	132.4 ± 20	146.6 ± 18	152.8 ± 32	−21.2 ± 6.6	−35.2 ± 4.9	−14.5 ± 4.6	4.6

[a]Band gap was determined by the surface plasmon resonance peak of the UV−vis spectrum.

area parameter. Two independent experiments were performed and presented as mean ± standard deviation (SD).

2.9.5. Dead/Live Assay. Live/dead assessment of the TiO_2 bulk- and TiO_2 nanoparticle-treated bacterial cells was done as per the protocol by Jung et al.[28] The treated bacterial culture was washed with PBS and incubated with PI (30 μM) and Syto 9 (20 μM) stains for 15 min at room temperature. The red fluorescence of PI was collected in the BL3 filter (647/10 band pass) of the cytometer, whereas the green fluorescence of Syto 9 was collected in the BL1 filter (530/30). The data were processed in FCS Express 5 software (Denovo, Los Angeles, CA), and the dead/live ratio was calculated and plotted as a graph by Graphpad Prism 5.

2.10. Microscopy. *2.10.1. Bright-Field Image Microscopy.* Bright-field microscopy was performed to analyze the morphological changes and other effects in HCT116 cells after treatment with TiO_2 bulk and TiO_2 nanoparticles at different concentrations for 24 and 48 h. The cells were seeded in a 24-well plate at a density of 1×10^5 cells/well and incubated at 37 °C and 5% CO_2 for 24 h. Following this, treatment was done, and the observation was taken as a picture with the help of an EVOS fluorescent microscope (AMG, Mill Creek, Washington). The microscope was attached with a Canon EOS 5D camera and the fluorescent filter of fluorescein isothiocyanate (green), PI (red), and 4′,6-diamidino-2-phenylindole (blue) excitation and emission range.

2.10.2. Fluorescence Microscopy. Fluorescence microscopy was done with the same microscope. For ROS determination in HCT116 cells, the cells were seeded and treated with TiO_2 bulk and TiO_2 nanoparticles on coverslips in a 24-well plate. Then, the cells were washed with chilled PBS and stained with DCFDA with incubation in the dark for 20 min. The images were observed and captured in the green channel of the microscope.

For the neutral lipid metabolism analysis in HCT116 cells, the treated cells were processed with a slight modification in the protocol, as described by Nioi et al.[29] Briefly, the cells were stained after fixation with 2% paraformaldehyde and permeabilization with 0.1% Triton X (Himedia, India). LipidTOX Deep Red neutral (Invitrogen) was used to stain the neutral lipid present inside the cells. The nuclei were stained with the Hoechst 33258 dye (blue).

Apoptosis assay in HCT116 cells was performed by fluorescent microscopy using the standard protocol of acridine orange (AO) staining.[30] TiO_2 bulk- and TiO_2 nanoparticle-treated cells were washed two times with PBS buffer and stained with 2 μg/mL AO/EtBr dissolved in PBS for 20 min. After staining, they were again washed two times to remove the extra stain. The images of the stained cells were then taken in the green and red channels of the microscope. The images were merged and presented.

2.10.3. In Silico Molecular Docking for TiO_2 Interaction. In silico investigation was carried out by molecular docking studies to determine the interaction of TiO_2 with different proteins involved in cellular metabolism. Molecular docking analysis was carried out by using AutoDock 4.2[31] using TiO_2 as the ligand and Sod1, p53, and VLDLR as receptor proteins. Chimera[32] was used to draw the structure of TiO_2, and the geometry was optimized by Gaussian 03 program. Energy minimization of the receptor proteins was done by using the Chimera program. The parameters for Ti were set for AutoDock 4.2. Grid dimensions were set to 40 × 40 × 40, with a spacing of 1 Å for all protein receptors with the help of Lamarckian genetic algorithms. Docking runs were performed by a genetic algorithm using a

DOI: 10.1021/acsomega.7b01522
ACS Omega 2018, 3, 1244−1262

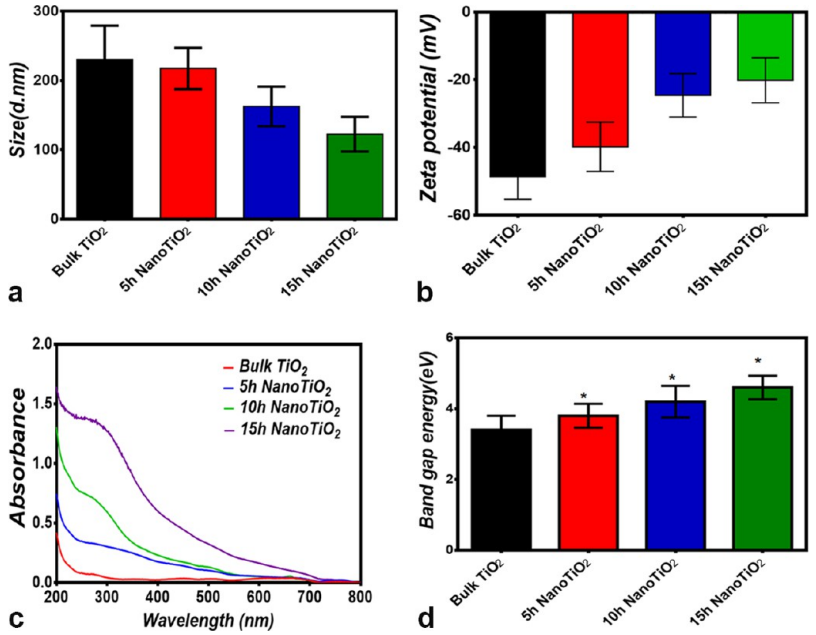

Figure 2. Characterization of TiO_2 nanoparticles prepared by the HEBM method. (a) Hydrodynamic diameter, (b) zeta potential, (c) UV−vis spectrum, and (d) band energy gap derived from the UV−vis spectrum. All parameters were determined for all four types of nanoparticles suspended in aqueous medium. Hydrodynamic diameter and zeta potential data are represented as mean ± SD of three independent measurements.

population size of 150 with the maximum number of evaluations set to 2 500 000 and maximal generations. The postdocking analysis was visualized by using Discovery Studio Visualizer. Two-dimensional interaction plots were derived from the receptor complexes having TiO_2 as a ligand by using LigPlot+.[33]

3. RESULTS

3.1. Synthesis and Physiochemical Characterization of TiO_2 Nanoparticles. Industrial synthesis of TiO_2 nanoparticles was mimicked on the lab scale by synthesizing them using the HEBM method.[34,35] Bulk TiO_2 particles, which were in the anatase phase, were milled, and 5, 10, and 15 h milled particles were collected. The collected nanoparticles were characterized for their physiochemical properties. No change in phase was observed after milling. As shown in Figure 1, field emission scanning electron microscopy (FESEM) was used to determine the size of nanoparticles, which confirmed the reduction of 105 ± 12 nm-sized bulk nanoparticles to 82 ± 14, 66 ± 12,, 42 ± 10 nm of 5, 10, and 15 h milled nano TiO_2 (Table 1). The hydrodynamic size of the synthesized TiO_2 nanoparticles was determined by DLS in all media (aqueous, PBS, and DMEM complete medium) used for the biological analysis, as mentioned in Table 1. It was found that increase in the milling time of the TiO_2 particles decreases the hydrodynamic size, as shown in Figure 2a. The size of the bulk TiO_2 particles was 268 nm (diameter), 269 nm, and 435 nm in aqueous, PBS, and DMEM medium, respectively, which was significantly reduced with milling time in all media (Table 1). Figure 2b showed that the zeta potential of bulk TiO_2 particles was −46, −67, and −32 mV in aqueous, PBS, and DMEM medium, respectively, which significantly increased with the milling time and was according to the standard value of dispersion of a suspension. The optical properties of the synthesized nanoparticles were determined by UV−vis spectroscopy. The band gap energy was also calculated as per the literature[36] report to confirm the change in the size of the synthesized TiO_2 nanoparticles. Figure 2c shows the blue shift in the absorption peak with the increase in the milling time of the TiO_2 particles. While calculating the band gap energy (Figure 2d), 15 h nanoparticles were found to be having the highest band gap (4.6 eV) in comparison to the 10, 5 h, and bulk particles, the band gap of which were 4.2, 3.8, and 3.4 eV (Table 1), respectively, and statistically significant.

3.2. In Vitro Cytotoxicity of Synthesized TiO_2 Nanoparticles. *3.2.1. Cellular Interaction of TiO_2 Nanoparticles with Mammalian Cell Lines.* Interaction of TiO_2 nanoparticles with HCT116 colon cells was investigated by determining the changes occurring at the cell membrane and cytoplasm because of TiO_2 bulk and TiO_2 nanoparticles. The effects were studied with the help of flow cytometry[27] by measuring the cellular uptake of nanoparticles and determining their surface charge potential.[37] Figure 3 shows the change in the zeta potential of HCT116 cells on interaction with TiO_2 nanoparticles at a concentration of 50 and 250 μg/mL for 24 and 48 h. Untreated cells were taken as the control. It was found that at a low

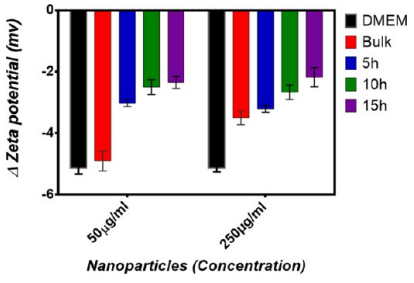

Figure 3. Change in the zeta potential of HCT116 colon carcinoma cell lines in the interval of 24−48 h exposed to bulk TiO_2 and nanoparticles, as determined by DLS. A significant gain in the zeta potential was observed in accordance with the milling time of TiO_2 nanoparticles both at low (50 μg/mL) and high (250 μg/mL) concentrations. Control cells were taken without any nanoparticle treatment.

DOI: 10.1021/acsomega.7b01522
ACS Omega 2018, 3, 1244−1262

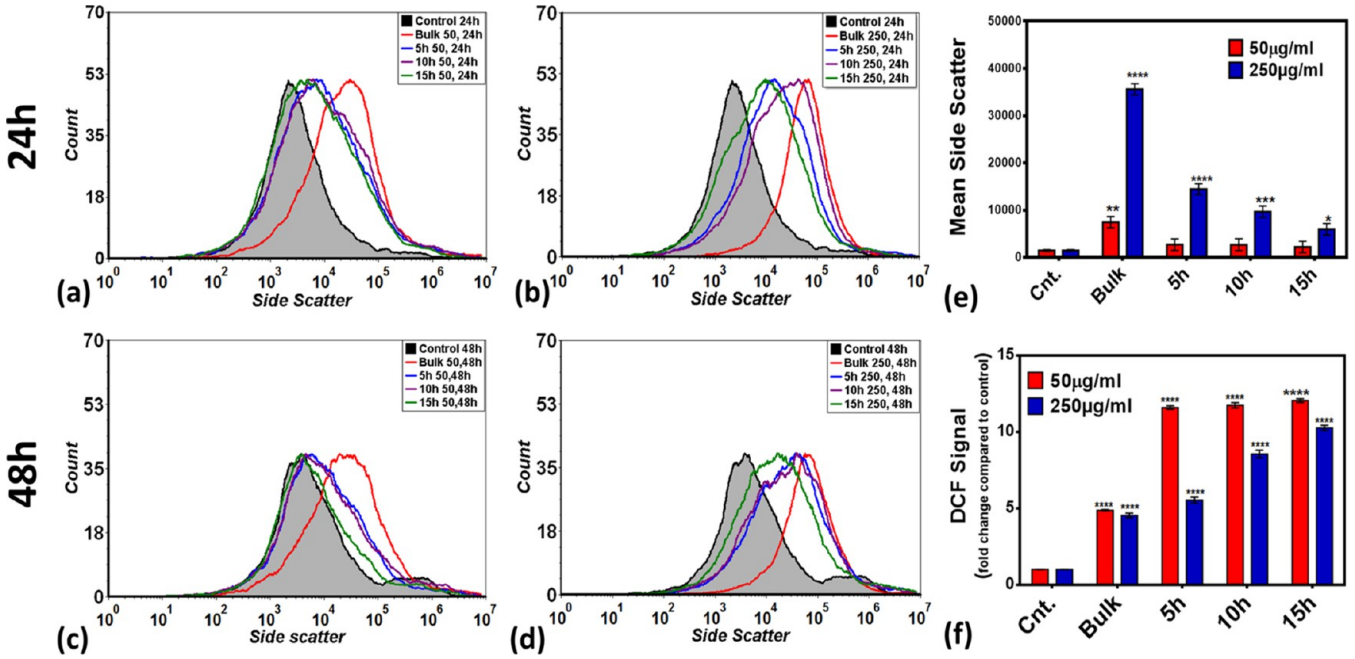

Figure 4. Granularity revealing the cellular interaction of TiO_2 nanoparticles by HCT116 cells treated for 24 and 48 h at low (50 μg/mL) and high (250 μg/mL) concentrations, as determined by flow cytometry. Side-scatter histogram of cells shifted toward left in accordance with the milling time; (a,b) present SSC of the exposed HCT116 cells for 24 h at 50 and 250 μg/mL; (c,d) present SSC for 48 h at 50 and 250 μg/mL; (e,f) represent the comparative view of the mean side-scatter of exposed HCT116 cells treated with TiO_2 nanoparticles with respect to cells with no exposure (control). The values present mean ± SD of three independent experiments. *P < 0.05 denotes the significant change from bulk particles and number of * presents the degree of significance.

concentration (50 μg/mL), the change in the zeta potential of HCT116 cell lines treated with 5, 10, and 15 h TiO_2 nanoparticles was less in comparison to the bulk TiO_2 particles. The same trends were observed at a high concentration (250 μg/mL), however, the change was −3.12 mV, much lesser than the low concentration in the case of bulk TiO_2 particles. Supporting Information Figure S1 reveals the measurement of zeta potential of HCT116 cell lines at 24 and 48 h at 50 and 250 μg/mL, where it was interesting to note that after 24 and 48 h of treatment, the zeta potentials of HCT116 cells were less or in line with those of the untreated cells in 5, 10, and 15 h TiO_2 nanoparticles, even though the cells treated with bulk particles have a higher zeta potential. To determine the uptake of nanoparticles by cells, the flow cytometry experimental procedure was followed, as described by Zucker et al.[27] The results shown in Figure 4a−d is in the form of a histogram representation of the side-scatter distribution of cells treated with TiO_2 bulk and TiO_2 nanoparticles at a concentration of 50 and 250 μg/mL for 24 and 48 h. These values were quantified by taking the mean side-scatter in the histogram (Figure 4e,f). The bulk particles were found to be showing the highest scattering in comparison to others with a decreasing trend with 5, 10, and 15 h milling time, respectively. Data showed that the side-scatter, representing the granularity of cells increases with the concentration, however, the interesting note to be taken is the decrease in the side-scatter of light with a decrease in the milling time and incubation period (24−48 h).

3.2.2. Cytotoxicity Evaluation of TiO_2 Nanoparticles. To study the cytotoxicity of TiO_2 bulk and TiO_2 nanoparticles, the viability of HCT116 cells treated with TiO_2 bulk particles and TiO_2 nanoparticles was first assessed in standard cell culture conditions by the MTT assay. Morphological change investigation by microscopy and depiction of the mechanism of cytotoxicity of TiO_2 nanoparticles by flow cytometry were done by ROS determination and apoptosis assays. As shown in Figure 5, it was clearly observed that the viability of cells

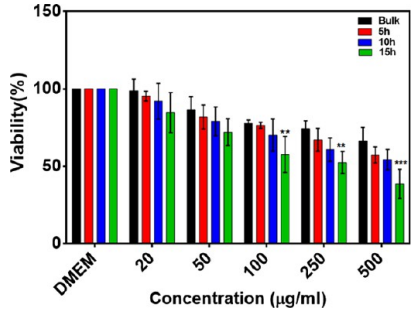

Figure 5. MTT viability assay for TiO_2 nanoparticle-treated HCT116 colon carcinoma cell lines. Data represented as the viability of cells. The y-axis presents the percentage viability as compared to the control. The x-axis denotes the concentration of nanoparticles. The different patterns of the bars represent the different types of TiO_2 nanoparticles obtained after collecting at different milling times. LC_{50} was obtained for each nanoparticle, which was found to be increasing with increase in the milling time. All experiments were done in triplicates and data were presented as mean ± SD of three independent experiments. *P < 0.05 denotes the significant change from bulk particles and number of * presents the degree of significance.

remains unaffected in bulk particles at a low concentration (20 μg/mL), however, the viability decreases significantly with a decrease in the size of particles obtained at different milling times. The survivability decreased up to 50% [lowest concentration of 50% viability (LC_{50})] in 15 h nanoparticles at 500 μg/mL, whereas it was higher in the case of 10, 5 h, and bulk particles. Bright-field imaging of HCT116 cell lines

DOI: 10.1021/acsomega.7b01522
ACS Omega 2018, 3, 1244−1262

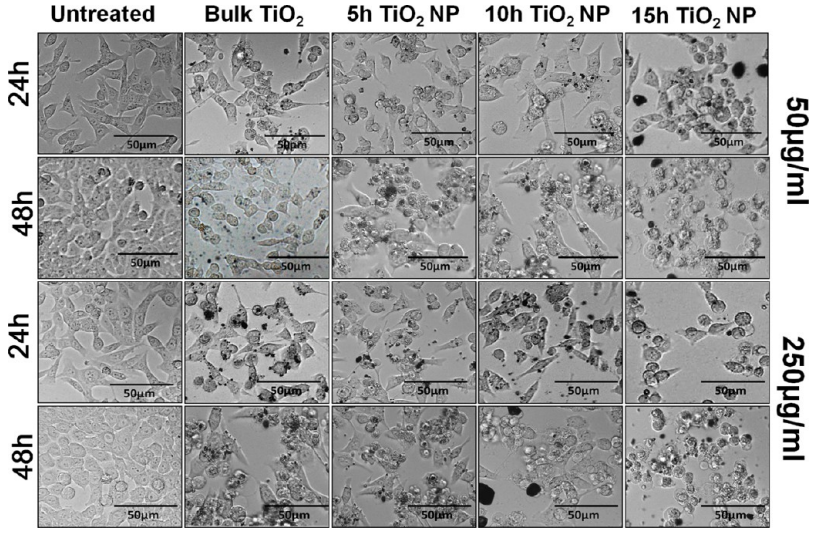

Figure 6. Optical micrographs of HCT116 cells treated with TiO_2 nanoparticles at 50 and 250 μg/mL exposed at 24 and 48 h.

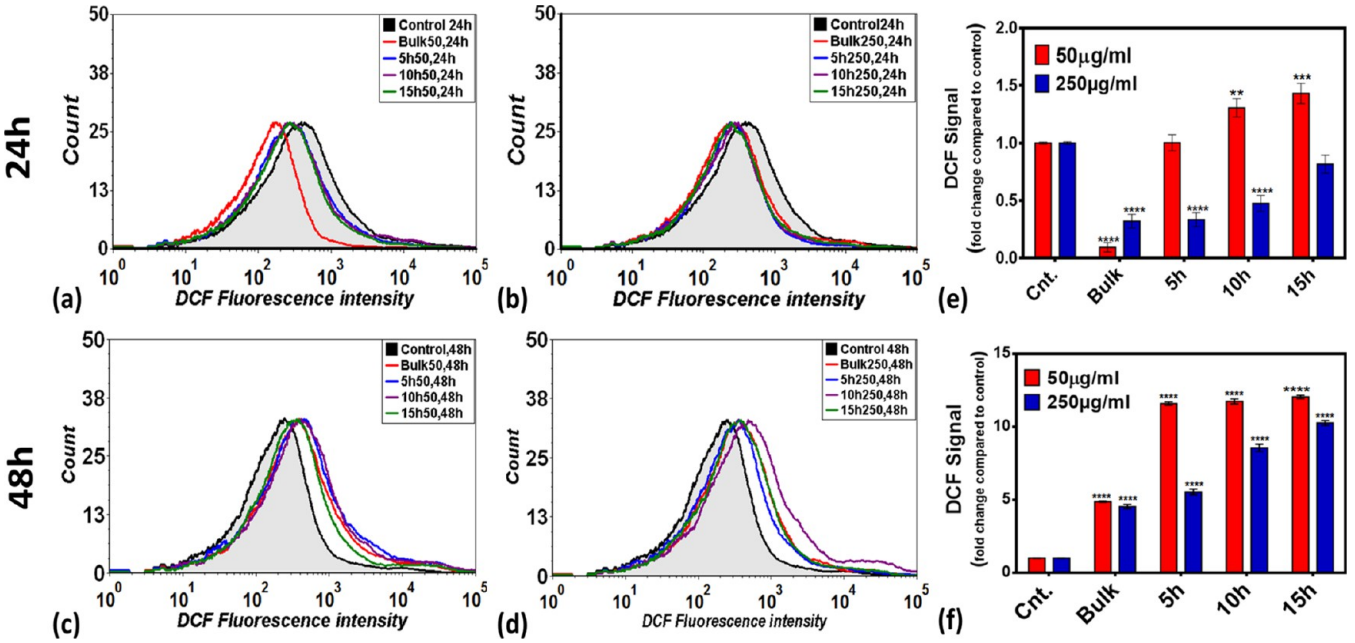

Figure 7. ROS measurement of HCT116 cells treated for 24 and 48 h at low (50 μg/mL) and high (250 μg/mL) concentrations, as determined by flow cytometry. Fluorescent intensity histogram of cells shifted toward left at 24 h and right at 48 h exposure in accordance with the milling time. (a,b) present the DCF fluorescent intensity of exposed HCT116 cells for 24 h at 50 and 250 μg/mL; (c,d) present the DCF fluorescent intensity of cells treated for 48 h at 50 and 250 μg/mL; (e,f) represent the comparative view of the fold change DCF signal intensity of the exposed HCT116 cells treated with TiO_2 nanoparticles with respect to cells with no exposure (control); the cells were stained with DCFHDA dye to measure ROS, which fluoresces green when reacting with ROS. The values represent mean ± SD of three independent experiments. *P < 0.05 denotes the significant change from bulk particles and number of * presents the degree of significance.

exposed to TiO_2 bulk and TiO_2 nanoparticles for 24 and 48 h was done keeping in view the LC_{50} of these particles to check the morphological differences in cells after treatment. Untreated colon cell lines HCT116 adhered to the cell culture plate surface uniformly in a spindle shape (Figure 6). Deformation of the cell membrane and nucleus was clearly observed to be enhanced at 48 h than 24 h exposure with adsorption of particulates of bulk, 5, 10, and 15 h TiO_2 nanoparticles to the outer membrane of the cells both at low (50 μg/mL) and high (250 μg/mL) concentrations, as shown in Figure 6. Moreover, the cells were found to have morphological changes and loss of attachment to the culture plate in exposed 5, 10, and 15 h TiO_2 nanoparticles at higher concentrations.

3.2.3. Evaluation of Oxidative Stress. Oxidative stress was analyzed by evaluation of ROS qualitatively and quantitatively by flow cytometry and fluorescent microscopy with the help of DCFDA in HCT116 cells treated with TiO_2 nanoparticles for 24 and 48 h. The analysis showed a significant decrease in the ROS production in cells treated with 50 and 250 μg/mL for 24 h (Figure 7a,b,e), however, it was found to be slightly increased when exposure was done for 48 h (Figure 7c,d,f). Interestingly, the ROS scavenging capacity of the nanoparticles was found to decrease with an increase in the milling time. Microscopic

DOI: 10.1021/acsomega.7b01522
ACS Omega 2018, 3, 1244−1262

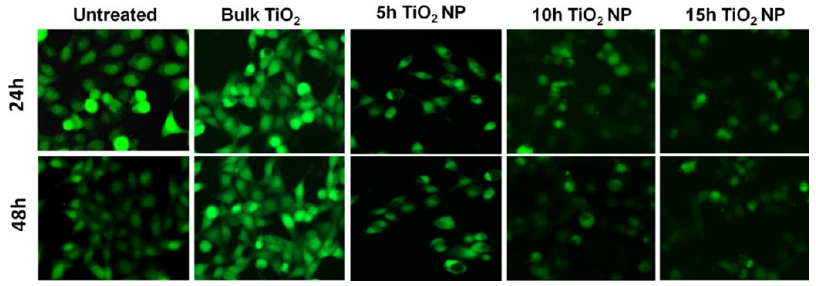

Figure 8. ROS determination of HCT116 cells treated for 24 and 48 h at 50 μg/mL concentration by fluorescent microscopy. Untreated and treated cells were stained with DCFDA after exposure for 24 and 48 h.

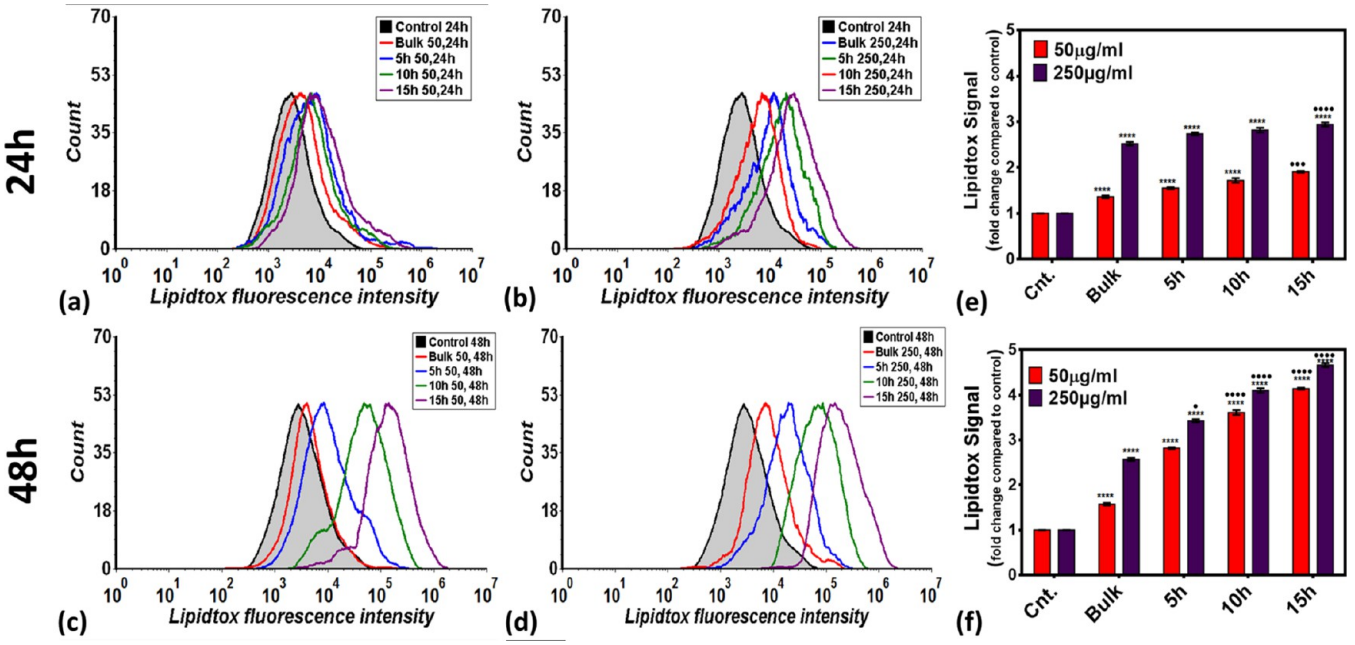

Figure 9. Neutral lipid measurement of HCT116 cells treated for 24 and 48 h at low (50 μg/mL) and high (250 μg/mL) concentrations, as determined by flow cytometry. Fluorescent intensity histogram of cells shifted toward left at 24 and 48 h exposure in accordance with the milling time. (a,b) present the LipidTOX fluorescent intensity of exposed HCT116 cells for 24 h at 50 and 250 μg/mL; (c,d) present the LipidTOX fluorescent intensity of cells treated for 48 h at 50 and 250 μg/mL; (e,f) represent the comparative view of the fold change LipidTOX signal intensity of the exposed HCT116 cells treated with TiO_2 nanoparticles with respect to cells with no exposure (control); the cells were stained with the Red neutral LipidTOX dye to measure lipid, which fluoresces red when combined with neutral lipids. The values present mean ± SD of three independent experiments. *$P < 0.05$ denotes the significant change from control cells and •$P < 0.05$ denotes the significant change from bulk particle-treated cells; number of * and • represent the degree of significance.

analysis of colon cells exposed to 50 μg/mL TiO_2 bulk and TiO_2 nanoparticles validated the flow cytometric analysis, as shown in Figure 8.

3.2.4. Evaluation of Steatosis Triggered by TiO_2 Nanoparticles. The accumulation of neutral lipids in HCT116 cell lines being exposed to bulk TiO_2 and TiO_2 nanoparticles (50 and 250 μg/mL) was evaluated by staining them with HCS LipidTOX Red neutral lipid stain and analyzing with the help of flow cytometry and microscopy. As shown in Figure 9, the fluorescent intensity was found to be the highest in cells treated with bulk particles and diminished with the increase in the milling time of particles both at 24 and 48 h exposure. Interestingly, 15 h TiO_2 nanoparticles showed half-fold increase in the fluorescent intensity at 48 h exposure. These data are well-supported by the microscopic images (Figure 10), where 15 h TiO_2 nanoparticles are found to possess lipids in a more clustered fashion than the untreated cells and the cells exposed to bulk, 5, and 10 h TiO_2 nanoparticles.

3.2.5. In Silico Analysis of TiO_2 Nanoparticle Interaction. To unveil the cytotoxic effect of TiO_2 nanoparticles in human colon cell metabolism on the molecular level, the computational approach was taken by performing molecular docking of proteins involved in oxidative stress (Sod1), lipid metabolism (VLDLR), and apoptosis (p53) regulation. As shown in Figure 11, AutoDock predicted TiO_2 nanoparticles hydrogen bond interaction with arginine (Arg), asparagine (Asn), and isoleucine (Ile) residues with Sod1 with bond lengths of 2.87, 3.27, and 3.13 Å, respectively. Hydrogen bond interaction of TiO_2 with p53 was also predicted with arginine (Arg), glycine (Gly), and serine (Ser) with bond lengths, whereas with VLDR, it was predicted with serine (Ser), threonine (Thr), and isoleucine (Ile). Pathway investigation through STITCH indicated the influence of TiO_2 on Sod1, p53, and VLDR by means of different catalysts and enzymes (Figure 12).

3.2.6. Genotoxic Effect of TiO_2 Bulk and TiO_2 Nanoparticles on HCT116 Cells. Genotoxicity of TiO_2 bulk and TiO_2 nanoparticles on HCT116 cells was determined by the

DOI: 10.1021/acsomega.7b01522
ACS Omega 2018, 3, 1244−1262

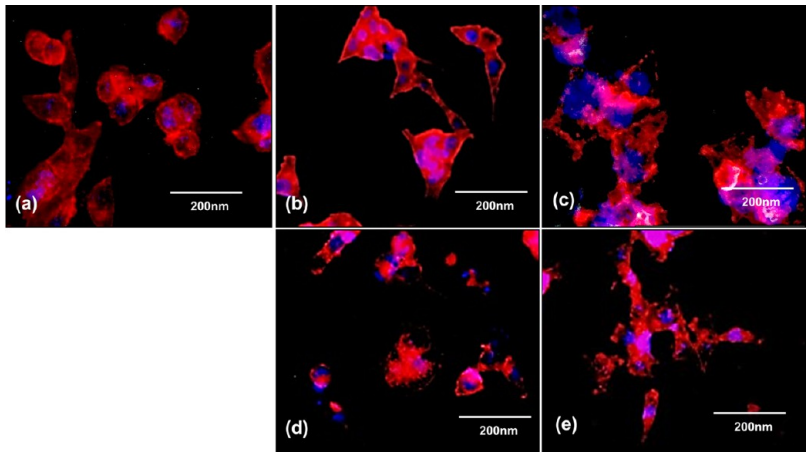

Figure 10. Fluorescent images of HCT116 cells stained with LipidTOX treated with TiO_2 nanoparticles at 50 μg/mL concentration. (a) Untreated cells. Images shown are HCT116 cell morphology treated with (b) bulk particles; (c) 5 h particles; (d) 10 h particles; and (e) 15 h particles. The cells were fixed, permeabilized, and stained with the Red neutral LipidTOX dye to measure lipid, which fluoresces red when combined with neutral lipids after treatment for 24 h.

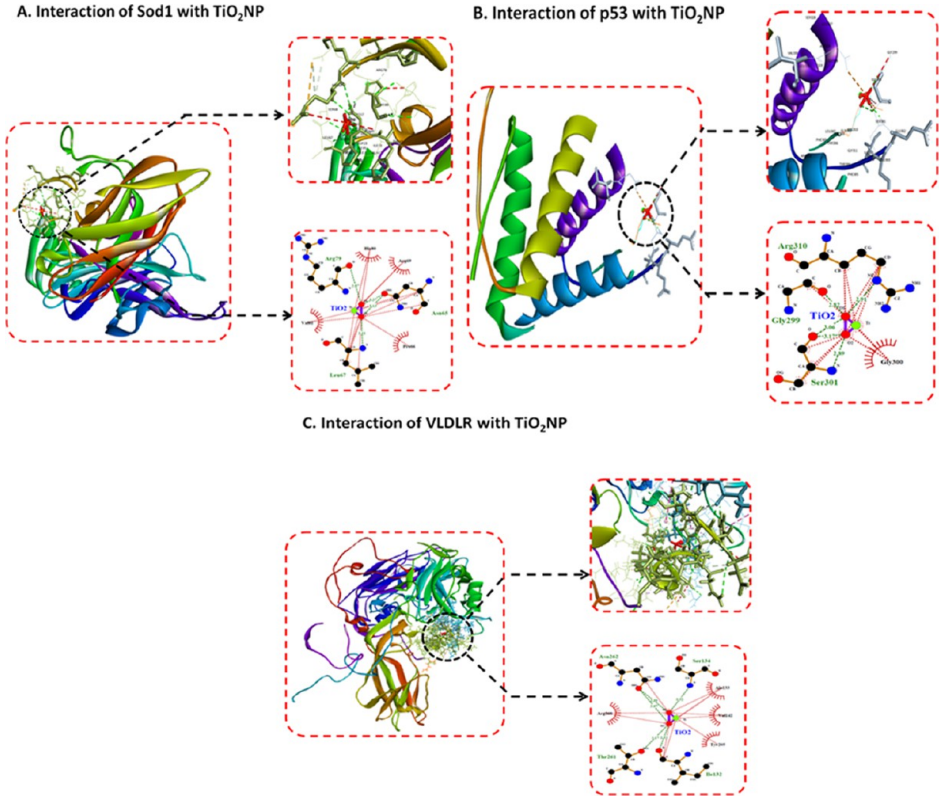

Figure 11. Molecular docking analyses of proteins with TiO_2 nanoparticles showing interacting residues using LigPlot+ and Discovery Studio Visualizer. (A) Sod1 with TiO_2, (B) p53 with TiO_2, and (C) VLDLR with TiO_2.

analysis of cell cycle and apoptosis of treated HCT116 cells. For the cell cycle analysis, statistical data from raw histograms (Figure S2) were extracted using FACS express 5 software, and the percentage of each phase was compared with the untreated cells and bulk TiO_2 particle-treated cells. The cell cycle nanoparticle-treated cells were found to be arrested at the G_0/G_1 phase with the increase in the TiO_2 nanoparticle concentration, however, bulk TiO_2 particles were arresting the cells at the S-phase (Figure 13). At a low concentration (50 μg/mL) and 24 h exposure, all nanoparticles were arresting cells at the G_0/G_1 phase. Interestingly, there was an increase in the S-phase cells exposed to 10 h milled nanoparticles from 10.36% at 24 h exposure to 14.56% at 48 h exposure, as compared to 8.28% in untreated cells. Moreover, the arrest was observed in the S-phase significantly along with the G_0/G_1 phase population increase at 48 h of exposure in 15 h milled TiO_2 nanoparticle-treated cells.

Further, apoptosis in TiO_2 bulk- and TiO_2 nanoparticle-treated HCT116 cells was analyzed by AO/EtBr staining. As shown in Figure 14, bulk TiO_2-treated cells were found to be in the late apoptotic phase, whereas the population of dead cells

DOI: 10.1021/acsomega.7b01522
ACS Omega 2018, 3, 1244−1262

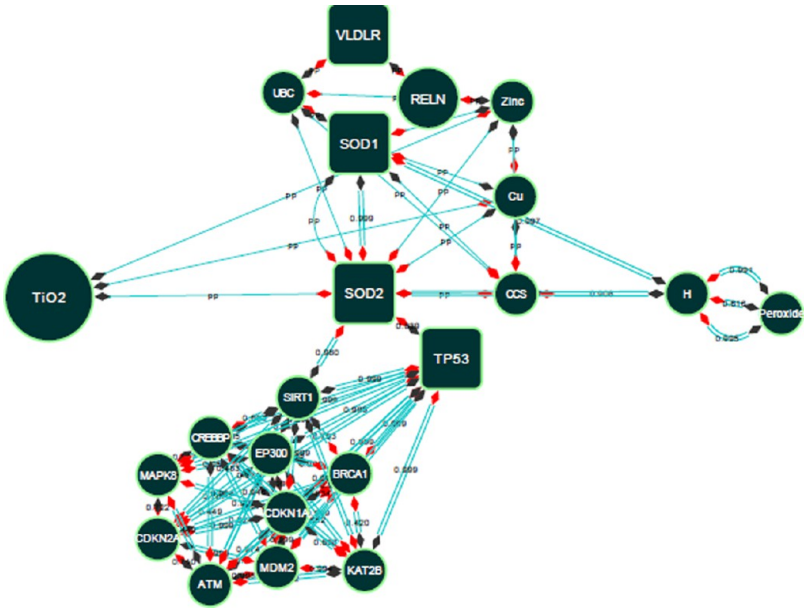

Figure 12. Pathway showing TiO_2 cytotoxicity mechanism involving interaction with Sod1, p53, and VLDLR proteins derived from STITCH and analyzed using Cytoscape.

with lost membrane integrity was enhanced in 5, 10, and 15 h milled TiO_2 nanoparticle-treated cells.

3.3. Antibacterial Activity of TiO_2 Bulk and TiO_2 Nanoparticles. *3.3.1. Bacterial Viability with TiO_2 Bulk and TiO_2 Nanoparticles.* Determination of antibacterial activity of TiO_2 bulk and TiO_2 nanoparticles was done by studying their interaction and effects with *S. typhimurium* and *E. coli*. The viability of bacterial strains was checked by live/dead staining with Syto 9/PI by flow cytometry. Live/dead assay results showed concentration- and size-dependent increase in the death of bacterial population after 4 h with negligible death in the control population in both the bacterial strains (Figure 15). At 50 μg/mL, bulk TiO_2 particles induced a 3.05% cell death in *E. coli*, which gradually increased to 3.96, 4.45, and 7.15% in 5, 10, and 15 h milled TiO_2 nanoparticles, respectively (Figure 15A). A similar trend was found with an increase in the concentration to 250 μg/mL with 10% increase, where the death of *S. typhimurium* population on the treatment of TiO_2 bulk and TiO_2 nanoparticles was similar to that of *E. coli*, however, the killing percentage was nearly 3% at 50 μg/mL concentration and varied only to 2 decimal places. The dead cell percentage got increased to 2 and 3 times, respectively, in 10 and 15 h milled nanoparticles at 250 μg/mL concentration (Figure 15B). The results revealed the increase in the antibacterial potency of TiO_2 nanoparticles with a decrease in the size.

3.3.2. Effect of TiO_2 Bulk and TiO_2 Nanoparticles on the Cell Membrane and the Oxidative Stress in Bacteria. The effect of TiO_2 nanoparticles on the cell membrane was investigated by determining the surface zeta potential of bacterial strains after treatment for 4 and 12 h with 50 and 250 μg/mL concentration. As shown in Figure 16, the magnitude of the zeta potential was found to be significantly enhanced from −15 mV to a range of −22 to −15 mV after immediate exposure of particles, which progressed in a decreasing manner with exposure time at both lower (50 μg/mL) and higher (250 μg/mL) concentrations. Moreover, the reduction was also observed to be dependent on the milling time of particles. Interestingly, the bacterial population exposed to 15 h nanoparticles was found to possess zeta potential close to that of the control population. Similar trends were observed in both the bacterial strains, however, the extent of reduction was drastically 5 times higher in the case of *E. coli* for bulk particles and 2−4 times greater for 5 and 10 h milled nanoparticles. Effect of ROS has been recognized to play an important role in the antibacterial properties of nanoparticles. Therefore, evaluation of ROS induction in both the bacterial strains *S. typhimurium* and *E. coli* was done on treatment with TiO_2 bulk and TiO_2 nanoparticles for 4 h. The evaluation was performed with the help of the flow cytometry technique using the fluorescent activity of the DCFDA dye. Data are represented in the form of a histogram, and the fold change in the DCF signal was calculated with respect to the control bacterial population (Figure 17). It was observed that the TiO_2 bulk and TiO_2 nanoparticles were behaving as a ROS scavenger; additionally, the left shift of the DCF fluorescent intensity from the control was the highest in 15 h milled nanoparticles. The trends were similar for both *S. typhimurium* and *E. coli* in 0 and 4 h incubation times. The findings were in line with the experimental results obtained from ROS evaluation in the HCT116 colon cancer cell line.

4. DISCUSSION

This study investigates the in vitro cytotoxicity of antibacterial TiO_2 nanoparticles synthesized as an industrial prototype. Cytotoxicity evaluation was done for TiO_2 nanoparticles synthesized by the ball milling technique with the HCT116 mammalian colon cell line.

4.1. Synthesis and Physiochemical Characterization of TiO_2 Nanoparticles. The TiO_2 nanoparticles were synthesized by the HEBM method by milling powdered bulk TiO_2 particles. HEBM is considered to be one of the standard methods for synthesizing nanoparticles both on the lab scale and on the industrial level.[35,38] The high energy produced by the mechanical force grinds the bulk particles, gradually reducing the size to nano level with an increase in the milling time.[39] Change in the physiochemical properties can be easily

DOI: 10.1021/acsomega.7b01522
ACS Omega 2018, 3, 1244−1262

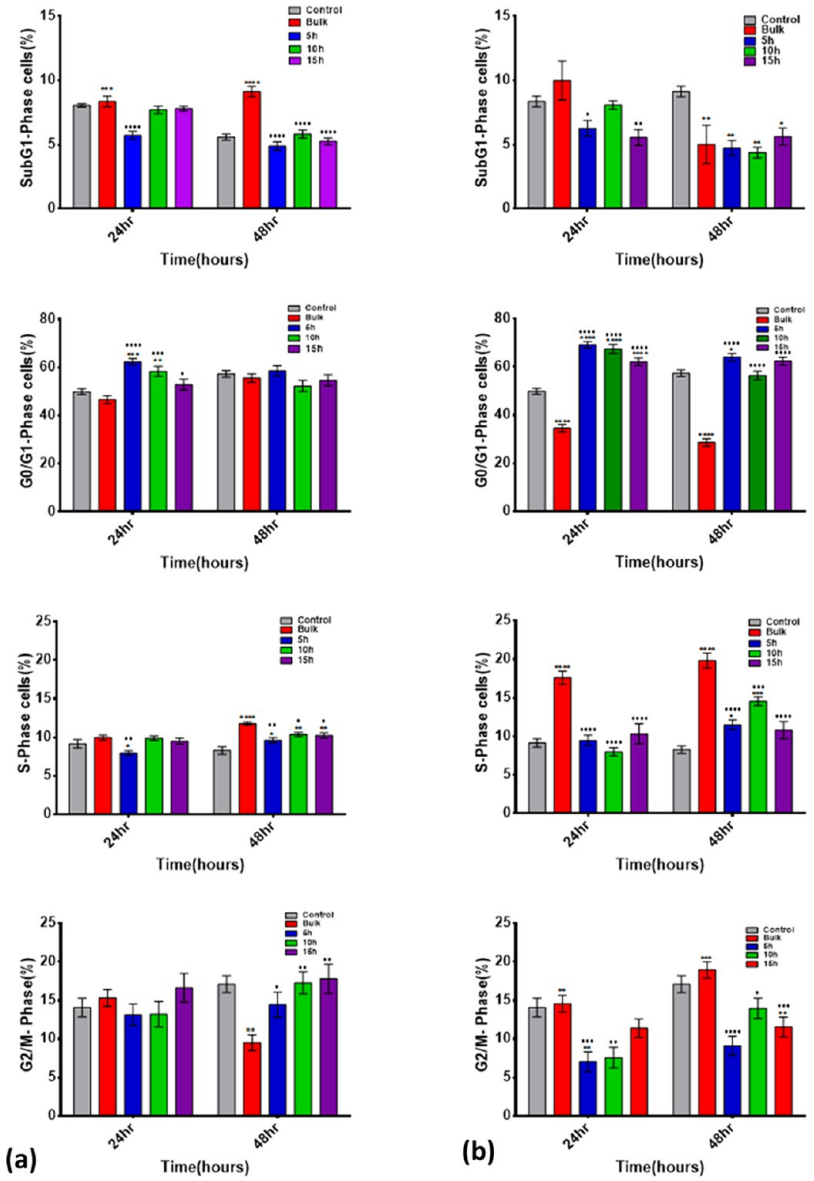

Figure 13. Histogram representation of the cell cycle of HCT116 cells treated with TiO_2 nanoparticles at (a) 50 and (b) 250 μg/mL concentrations. Cell cycle analysis showed that nanoparticles of 5, 10, and 15 h arrest the cell cycle at G_0/G_1 in contrast to the bulk particles, which arrests them at the S-phase. Phase arresting was dependent on concentration and time of exposure. The values represent mean ± SD of three independent experiments. *$P < 0.05$ denotes the significant change from control cells and •$P < 0.05$ denotes the significant change from bulk particle-treated cells; number of * and • represent the degree of significance.

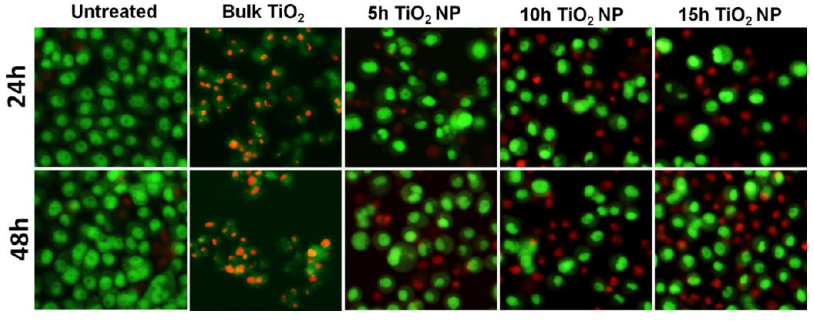

Figure 14. Fluorescent images of HCT116 cells stained with AO/EtBr treated with TiO_2 nanoparticles at 50 μg/mL concentration.

visualized and confirmed by different characterization techniques. In this study, synthesis of TiO_2 nanoparticles was done on the lab scale by using high-energy milling for different hours (5, 10, and 15 h). The particles were characterized by their physiochemical properties such as the size and zeta potential. FESEM analysis confirmed the reduction of bulk TiO_2 size up

DOI: 10.1021/acsomega.7b01522
ACS Omega 2018, 3, 1244−1262

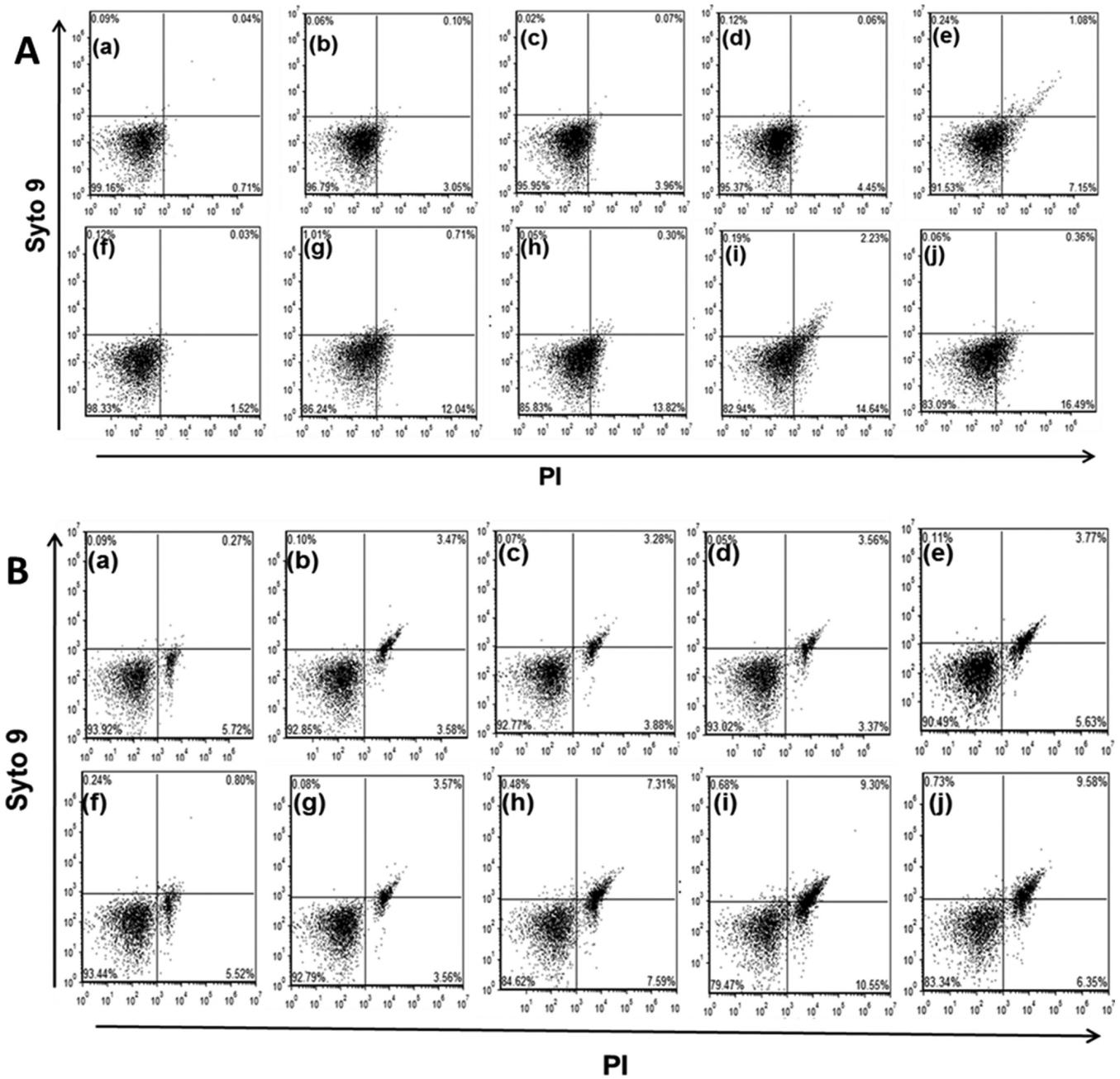

Figure 15. Live/dead assay of bacteria in the presence of TiO_2 bulk and TiO_2 nanoparticles for 0 and 4 h, as obtained from flow cytometry. (A) Dot plot of *E. coli* live/dead assay: (a,f) represent untreated cells at 0 and 4 h. Nanoparticle-treated cells are presented as (b,g) bulk; (c,h) 5 h; (d,i) 10 h; and (e,j) 15 h treated at 0 and 4 h, respectively. (B) Dot plot of *S. typhimurium* live/dead assay: (a,f) represent untreated cells at 0 and 4 h. Nanoparticle-treated cells are presented as (b,g) bulk; (c,h) 5 h; (d,i) 10 h; and (e,j) 15 h treated at 0 and 4 h, respectively. Analysis showed that the death of bacterial cells increased in accordance with time and increase in the milling time of the bulk particles.

to 40 nm on 15 h milling. The experiments for the evaluation of cytotoxicity and antibacterial efficacy of the nanoparticles were performed in a specific medium (PBS and complete DMEM), so it was important to determine the physiochemical properties of the TiO_2 nanoparticles such as the size and charge in the corresponding medium.[40] Reduction of the hydrodynamic diameter of the TiO_2 particles was found with an increase in the milling time, as shown in Figure 2a, in all media. The data demonstrated that the agglomeration tendency of the TiO_2 nanoparticles decreases with an increase in the milling time and varied according to the medium. The agglomeration of the nanoparticles also depends on the degree of repulsion between the particles inside the medium.[41] To estimate this, the zeta potential of each nanoparticle was determined, which is a measure of the electrokinetic potential to depict the degree of repulsion. Previous reports have defined zeta potential as a function of the nanoparticle size in different media by means of an effect of interaction between the particle surface and medium molecules affecting the surface ionization and henceforth the dispersion stability of particles.[41,42] Figure 2b shows that the zeta potential significantly increases with the milling time and is according to the standard value of dispersion of a suspension.[43] The probable explanation of the observed results can be attributed to the decrease in the surface area due

DOI: 10.1021/acsomega.7b01522
ACS Omega 2018, 3, 1244−1262

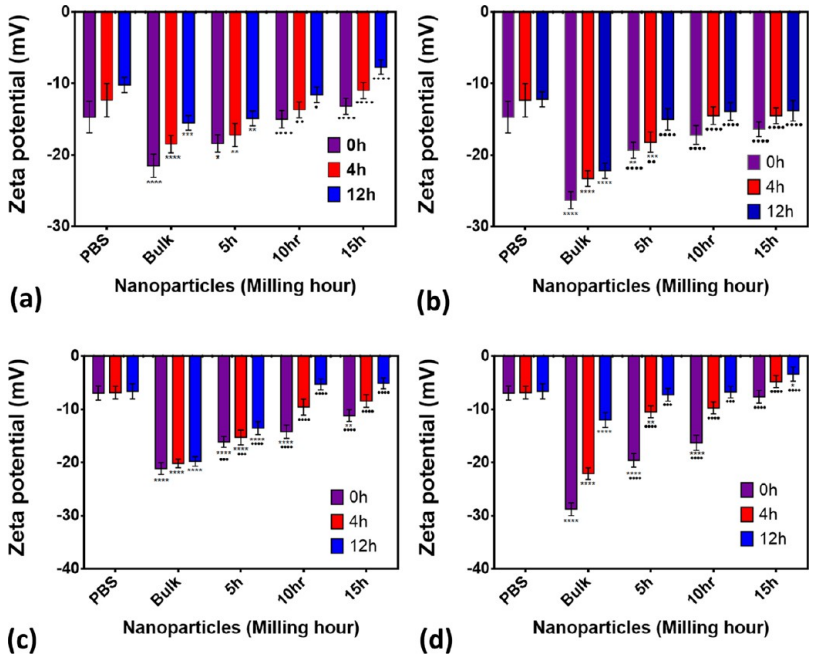

Figure 16. Zeta potential of *S. typhimurium* (a,b) and *E. coli* (c,d) treated with TiO_2 bulk and TiO_2 nanoparticles at 0, 4, and 12 h, as determined by DLS. A significant gain in the zeta potential was observed in accordance with the milling time of TiO_2 nanoparticles both at low (50 μg/mL) (a,c) and high (250 μg/mL) (b,d) concentrations. The untreated cells were taken without any nanoparticle treatment. All data represent mean ± SD of three independent experiments. *P < 0.05 denotes the significant change from untreated cells and •P < 0.05 denotes the significant change from bulk particles-treated cells; number of * and • represent the degree of significance.

to a decrease in the size with constant pK_a of the medium.[41] The alteration in the shape and size of the nanoparticles because of milling causes an increase in surface structure imperfections, especially oxygen vacancies, leading to a change in the electronic structure of the particle. These vacancies are then occupied by the adsorption of the −OH group of water molecules, producing a positive charge. The intensity of adsorption enhances with an increase in the oxygen vacancies, thereby increasing the positivity in the zeta potential.[44,45] These results indicated that the nanoparticles were in dispersed suspension in all media, however, the variation in the hydrodynamic size and zeta potential in different media can be attributed to the presence of salts and other molecules in different media.[43] It has been reported that the presence of different salts and molecules defines the physiochemical nature of the nanoparticles, which plays an effective role in the cytotoxicity and genotoxicity of nanoparticles in different biological studies.[46] The optical property of the synthesized nanoparticles was estimated by UV−vis spectroscopy, which is a strong technique to characterize nanoparticles with respect to their light absorption properties. Figure 2c shows the blue shift in the absorption peak with increase in the milling time of the TiO_2 particles. Band gap energy was found to increase with an increase in the milling time depicting their reduction with a decrease in the size. Smaller particle size refers to a larger band gap because fewer molecular orbitals are being added to the possible energy states of the particle. Hence, absorption will occur at higher energies, so a shift toward shorter wavelengths will be apparent. Synthesis of metallic oxide nanoparticles such as ZnO has been reported by HEBM in previous studies.[47] Similar changes in physiochemical properties of ZnO nanoparticles have been reported in the case of zinc oxide in the previous literature reported by our group and other groups.[47−50] These results have revealed the change in physiochemical properties of TiO_2 nanoparticles with milling time and speculated their change in the biological effect accordingly.

4.2. In Vitro Cytotoxicity of Synthesized TiO_2 Nanoparticles. Cytotoxicity is the primary biological end point in evaluating the toxicity of environmental contaminants. In vitro cytotoxicity of nanoparticles relies upon their interaction and its consequences on physiological and genetic metabolic processes. Nature of interaction of nanoparticles with the cells decides the toxicological behavior of the nanoparticles. The nanoparticle interacts with cells, resulting in a change in their cytoplasm[27,51] as well as on their surface.[52] These effects can be studied by flow cytometry[27] by measuring the cellular uptake of nanoparticles and determining their surface charge potential.[46] Figure 2 shows the milling time-dependent change in the zeta potential of HCT116 cells on interaction with TiO_2 nanoparticles at a concentration of 50 and 250 μg/mL for 24 and 48 h. The zeta potentials of HCT116 cells were less or in line with the untreated cells in 5, 10, and 15 h milled TiO_2 nanoparticles after 24 and 48 h exposure. These results suggest that the surface charge of HCT116 cell lines are affected because of the size and intensity of accumulation of the bulk and nanoparticles on the surface. The zeta potential of the particle adds to the surface charge of cells, leading to an increase in the total zeta potential at 24 and 48 h. However, it can be speculated that at 48 h exposure, the uptake of nanoparticles inside the cells plays an important role in the decreasing behavior of the surface zeta potential of HCT116 cells, which have to be determined experimentally. These findings are in correlation with the studies done by Zhang et al.[53] Uptake analysis by flow cytometry revealed an increase in the side-scatter (90° direction) of the cells after treatment of cells with TiO_2 bulk and TiO_2 nanoparticles. Side-scatter is regarded as the indicator of granularity and mass of cells.[54] Previous reports have

DOI: 10.1021/acsomega.7b01522
ACS Omega 2018, 3, 1244−1262

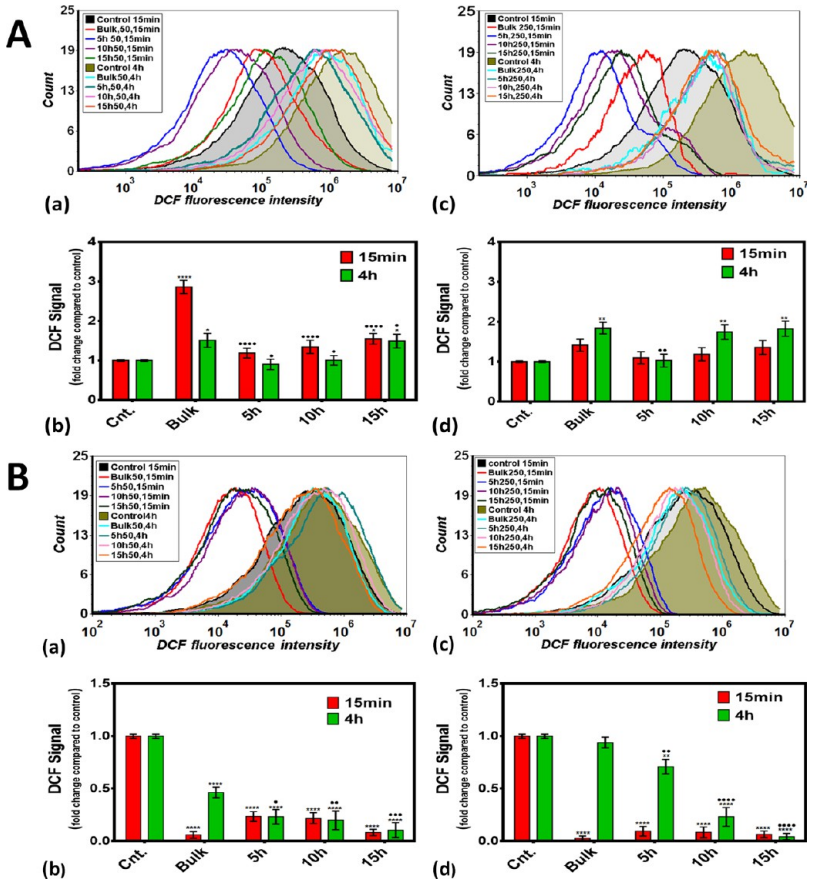

Figure 17. ROS measurement of bacterial strains treated with TiO_2 nanoparticles. (A) *S. typhimurium* and (B) *E. coli* treated for 0 and 4 h at low (50 μg/mL) and high (250 μg/mL) concentrations, as determined by flow cytometry. Fluorescent intensity of cells shifted toward left at immediate exposure, that is, 0 h as well as at 4 h exposure in accordance with the milling time. (a,b) represent the DCF fluorescent intensity and fold change DCF signal intensity of exposed bacterial cells at 50 μg/mL; (c,d) present the DCF fluorescent intensity and fold change DCF signal intensity of exposed bacterial cells at 250 μg/mL. DCF fold change was calculated with respect to cells with no exposure (control); the cells were stained with the DCFHDA dye to measure ROS, which fluoresce green when reacting with ROS. The value represents mean ± SD of three independent experiments. *$P < 0.05$ denotes the significant change from bulk particles and number of * represents the extent of significance.

described the side-scatter change in relation with electron microscopy (high-resolution transmission electron microscopy)[55] and fluorescent microscopy[56] as an effective tool to determine the uptake of nanoparticles inside cells.[57] In this study, the signal appeared to be a result of both internalized and surface-adsorbed particles, which causes the variation in the side-scattering of light. The bulk particles were found to be showing the highest scattering in comparison to others with a decreasing trend with 5, 10, and 15 h milling time, respectively. The relationship of concentration of nanoparticles with their uptake has been described by many groups.[58] The results are in correlation with those descriptions emphasized with the milling time and incubation period.

The findings indicate that the size and agglomeration vary with the milling time of the TiO_2 particles and play an important role in their cellular interaction. The bulk particles having the highest hydrodynamic diameter and lowest zeta potential when milled for 5, 10, and 15 h lead to a decrease in the size as well as an increase in the zeta potential. There is a consequent increase in the zeta potential and a decrease in the granularity of HCT116 cell lines treated with these particles. A study by Zhang et al.[53] showed the modulation of the zeta potential of the mammalian cell via nanoparticle incubation and explained the uptake of nanoparticles by cells as a function of the zeta potential. Our studies were following the same trends with TiO_2 nanoparticles and HCT116 cells. Consequently, nanoparticle uptake can be explained with a two-step process: binding with the plasma membrane followed by internalization. The attachment of negatively charged bulk TiO_2 and TiO_2 nanoparticles on the cell plasma membrane causes the increase in the zeta potential. The internalization process, however, results in a change in the zeta potential in a reverse way because of vesicular transport-based cell endocytosis. The zeta potential of cells that interacted with the bulk particles was less at 24 h than at 48 h, which can be due to more attachment with the cell plasma membrane with time. However, the change in the zeta potential by 5, 10, and 15 h as compared to that of the bulk particles was following the same increasing trend both at low and high concentrations (50 and 250 μg/mL). This defines the zeta potential as a factor of nanoparticle attachment to the cell membrane. Further attachment leads to the trends in the variation of the side-scatter intensity in flow cytometry. The possible nature of the trend of increase and decrease in side-scatter with the size (milling time) of the nanoparticles and the incubation period (Figure 4a,b) could be explained by the following reasons: First, the bulk and nanoparticle attachment to the cell surface plasma membrane changes the zeta potential value of the cells, thereby causing accumulation on the surface because of charge interaction.[59,60] This surface adsorption leads to an increase in the scattering of light. As the size and zeta

DOI: 10.1021/acsomega.7b01522
ACS Omega 2018, 3, 1244−1262

potential of the bulk particles were the highest among others, the interaction was the highest, leading to more scattering. The properties decreased with the size of the particle and hence there was lowest scattering by 15 h nanoparticles. Second, the granularity change of the cell cytoplasm, as indicated by the change of light scattering because of the nanoparticle internalization, could be attributed to the vesicular transport-based cell endocytosis. During endocytosis, the uptake of particles attached to the cell surface takes place by invagination and formation of the new intracellular vesicle,[61] thus losing a small portion of the cell membrane and leading to a decrease in the negative charge. The extent of internalized nanoparticles depends on the accumulation of particles on the surface of the cell plasma membrane. Because 15 h nanoparticles have the least accumulation, lowest scattering and granularity was found. The phenomenon was consistent and directly proportional to the time of incubation and concentration of nanoparticles. Studies by Prasad et al.[43] showed that the cellular interaction of nanoparticles is a function of agglomeration of nanoparticles in the medium. Our results were in line with those reports and additionally show their effect on the uptake and granularity of HCT116 cells.

As analyzed by the MTT assay and morphological change determination, the viability of cells was found to be dependent on the milling time and concentration of the TiO_2 bulk and TiO_2 nanoparticles. The results were in correlation with the flow cytometry uptake experiment results, suggesting a reduction in cell activity and even cell death after 24 and 48 h exposure with TiO_2 bulk and TiO_2 nanoparticles. These results were in agreement with some reports[62] and in disagreement with others[63] on the cytotoxicity of TiO_2 nanoparticles. The conflict in idea may be due to the difference in specificity of the mechanism of assays by which cytotoxicity is evaluated, such as mitochondrial function (MTT assay) versus membrane permeability (live/dead, trypan blue assay). Recently Wang et al.[61] explained the cause of cytotoxicity of TiO_2 nanoparticles as the hindrance of ion exchange leading to a disruption of exocytosis processes due to the accumulation of excess TiO_2 nanoparticles on the cell surface. Our results were in agreement with them explaining the cytotoxic behavior of TiO_2 bulk and TiO_2nanoparticles because of their cell surface attachment.

Many reports have suggested the role of ROS as an important factor for the cytotoxicity of TiO_2 nanoparticles.[64] ROS evaluation with bulk and synthesized TiO_2 nanoparticles with HCT116 indicated toward their milling time-dependent ROS scavenging property. It was revealed that the particles were scavenging the peroxide molecules, which were produced intensively during 24 h exposure. However, the generation of ROS was there even after 48 h exposure. This observation can be attributed to the complete consumption of the internalized TiO_2 nanoparticles for scavenging of ROS molecules during 48 h exposure. This effect may be due to the interaction between the unpaired electrons of free radicals and the conduction band electrons of the metal nanoparticles. These results are in contrast with the existing studies about TiO_2 nanoparticles cytotoxicity studies.[65] Literature has defined TiO_2 nanoparticles as an oxidative stress-inducing agent by ROS generation and damaging of their scavenger molecules inside the cytoplasm, leading toward influence on the respiratory chain and cell death.[66] By contrast, our results revealed that TiO_2 bulk and TiO_2nanoparticles act as the ROS scavenger inside the cytoplasm. One possible explanation for this intriguing fact is the presence of oxygen vacancy.[67] Metal oxide nanoparticles prepared by the ball milling method and other techniques have been reported to possess oxygen vacancy as their intrinsic defects by many researchers.[7] These oxygen vacancies are the points in the lattice where an electron is missing from the oxygen shell. Such oxygen vacancies react with the free electrons of free radicals leading to an antioxidant property similar to that of the reported oxide nanoparticles such as cerium oxide and zirconium oxide.[68] In silico investigation, as shown in Figure 11, showed the interaction of the oxygen atom of TiO_2 with amino acid residues. Discrepancy of fact can be reasoned as the inability of synthesized TiO_2 nanoparticles to interact with Sod1 because of the lack of the oxygen atom.

Steatosis refers to the intracellular abnormal retention of neutral lipids inside the cells, which are often triggered by factors that affect the metabolism of fatty acid and/or neutral lipids. The accumulated neutral lipids follow the toxic side effects of the drugs.[69] Nanoparticles have been found to trigger steatosis leading to the toxicological effect such as induction of hypoxia-inducible transcription factor 1α (HIF-1α). The HIF family regulates the adaptation to hypoxic condition critical for cell survival.[70] Estimation of neutral lipids in HCT116 cells triggered by TiO_2 bulk and TiO_2 nanoparticles revealed diminished steatosis with increasing milling time. The accumulation of lipids in cytoplasmic LDs in HCT116 cells lines has not been reported previously, however, the phenomenon has been reported in PC12 glial cells on exposure to $CoCl_2$ nanoparticles.[71] LDs have been described reliably as a dynamic organelle, which participates in the important function of cells, such as transport and communication, by communicating with other cellular compartments inside the cell.[72] Accumulation of lipids has been found as a consequence of disturbance of the cellular membrane on the cell surface as well as cellular malfunction inside the cells.[71] With reference to these reports and our experimental observation, a possible explanation of accumulation of the neutral lipids on exposure to TiO_2 bulk and TiO_2 nanoparticles could be the release of free (unesterified) fatty acids as a result of distortion of the cellular membrane, which forms triacylglycerol (the main components of LDs). Moreover, the abnormalities in the functionality of VLDR proteins because of an oxygen vacancy in TiO_2 can also be accused of the reason, as revealed by the computational investigation (Figure 11). These accumulated LDs could influence the mitochondrial function, which might cause oxidative stress, leading to a probable cause of cytotoxicity.

Studies on the ROS analysis and lipid analysis indicated the effect of bulk TiO_2 and TiO_2 nanoparticles in the cytoplasm, however, their genotoxicity effect is an important aspect to be studied. TiO_2 nanoparticles have been reported to induce an alteration in the cell cycle in different mammalian cell lines.[73] The cell cycle is a series of events that lead to cell division and replication. It commences with the G_1 phase, in which the cell increases its size, followed by S, G_2, and M phases, where the synthesis of DNA, preparation for division, and division take place, respectively. Cells with damaged DNA will be arrested in any of these phases depending on the intensity of damage, however, cells with irreversible damage will undergo apoptosis and accumulate in the sub-G_1 phase.[74] The effect of TiO_2 bulk and TiO_2 nanoparticles on the cell cycle of HCT116, as analyzed by flow cytometry, revealed the milling time- and concentration-dependent arresting of the cell cycle at S and G_0/G_1 phases. These findings referred the influence of TiO_2 nanoparticles on the synthesis of DNA as well as a delay in

DOI: 10.1021/acsomega.7b01522
ACS Omega 2018, 3, 1244−1262

the progress of the cell cycle to the next stage. It may be speculated that there may be the role of interaction of TiO_2 bulk and TiO_2 nanoparticles with proteins taking part in the process of synthesis, which needs to be investigated in detail. Apoptosis analysis showed (Figure 12) the consequent effect of the cell cycle arrest in treated cells. Cells exposed to bulk TiO_2 particles were found to be in the late apoptotic phase, whereas the number of membrane distorted and dead cells increases with milling time and exposure to TiO_2 nanoparticles. The observation can be attributed to the increase in the cell cycle arrest as a result of cytotoxicity. Moreover interaction of TiO_2 particles with the protein responsible for apoptosis can also be reasoned for the phenomenon. p53 has been reported to play a key role in apoptosis.[75] Computational results, as shown in Figure 11, show the interaction of TiO_2 with amino acid residues of p53, which can be attributed to the abnormal functionality of p53 leading to apoptotic results. The overall corridor of cytotoxicity exhibited by TiO_2 bulk and TiO_2 nanoparticles can be interpreted by the pathway shown in Figure 12 displaying the role of catalysts and proteins. These results may mimic a real world exposure of commercially prepared TiO_2 nanoparticles to intestinal cells more than the standard in vitro studies because of the intake of TiO_2 nanoparticles through food or water.

4.3. Antibacterial Activity of TiO_2 Bulk and TiO_2 Nanoparticles. TiO_2 nanoparticles have been recognized widely as an antibacterial agent. Many researchers have studied their effect on different pathogenic as well as nonpathogenic bacterial strains.[76] TiO_2 nanoparticles used in day-to-day life products such as cosmetics, sunscreen, food products, paints, and so forth are industrially prepared by the ball milling method; hence, the antibacterial properties of these nanoparticles need to be studied. In this study, the interaction of TiO_2 nanoparticles prepared by the mechanical milling of bulk TiO_2 particles as an industrial prototype method was investigated with commonly occurring bacterial strains such as *S. typhimurium* and *E. coli*. Live/dead assay results showed concentration- and size-dependent increase in the death of bacterial population after 4 h treatment, with negligible death in the control population of both the bacterial strains (Figure 13). The results revealed the increase in the antibacterial potency of TiO_2 nanoparticles with the decrease in the size. Dependence of antibacterial activity on the size and charge of nanoparticles has been described recently by many groups.[77] Our results were in line with these studies and provided a concrete evidence of the described phenomenon with respect to TiO_2 nanoparticles prepared by the HEBM method. Conferring to the effect of TiO_2 nanoparticles on the surface charge of the mammalian cell line, we presumed that the effect of TiO_2 nanoparticles on the surface charge of bacterial strains would have been playing an important role in their killing. To evaluate our assumption, the zeta potential of *S. typhimurium* and *E. coli* was checked after 4 and 12 h of treatment with 50 and 250 μg/mL of TiO_2 bulk and TiO_2 nanoparticles. Zeta potential was found to be elevated with decreasing size and increasing exposure time of TiO_2 nanoparticles (Figure 14). These data validated the speculated presumption of nanoparticles exposure effect on the surface of the bacterial cell. Though there are reports on the toxic effect of TiO_2 nanoparticles in bacteria and their possible cause, there is a gap of information regarding the role of effect on the membrane. Recently Arakha et al.[24] had explained the vitality of nano−biointerface for the antibacterial propensity of iron oxide nanoparticles and suggested the role of surface zeta potential in determining the antibacterial activity. Moreover, studies reported by Tang et al.[25,78] have mentioned the effect of bacterial killing as a consequence of attachment of titanium oxide nanoparticles and its composites to the bacterial surface, leading to protein denaturation and cell death. The data presented in this study substantiate those findings with regard to prepared TiO_2 nanoparticles. With reference to the findings of the previous literature and the results obtained, it can be argued that the difference in the magnitude of prepared TiO_2 and bacterial surface zeta potential forming a gradient leads to attachment of nanoparticles to the bacterial surface. Rise in the gradient zeta potential with the milling time of TiO_2 nanoparticles enhances the attachment, leading to higher antibacterial efficiency in 5, 10, and 15 h nanoparticles. Investigation of the mechanism of antibacterial activity was further carried by the oxidative stress analysis in TiO_2 bulk- and TiO_2 nanoparticle-exposed bacterial cells. Figure 15 shows the exposure- and milling time-dependent ROS scavenging activity of bulk TiO_2 and TiO_2 nanoparticles. Previous reports have mentioned ROS as the key role of the mechanism of bacterial killing due to exposure of nanoparticles.[79] The findings were similar to experimental results obtained from ROS evaluation in the HCT116 colon cancer cell line and provided concrete evidence for the explanation of the presence of oxygen vacancy in TiO_2 bulk and TiO_2 nanoparticles leading to their ROS scavenging property in living cells. Many literature reports have suggested other reasons for the antibacterial property of nanoparticles such as disruption of the cell membrane,[78,80] dysfunction of cell organelles,[81] and DNA damage[82] in bacterial cells. The actual cause is still undiscovered and needs detail investigation.

In reference to the above studies, mechanically synthesized TiO_2 nanoparticles were found to have antibacterial effects against *S. typhimurium* and *E. coli* with a contradiction of the ROS scavenging antibacterial mechanism.

5. CONCLUSIONS

In summary, we have elucidated the impact of industrially synthesized TiO_2 bulk and TiO_2 nanoparticles used in daily market products on the cytotoxicity of the colon cancer cell line (HCT116). We also demonstrated their antibacterial activities on *E. coli* and *S. typhimurium*. TiO_2 nanoparticles prepared by the HEBM method as the industrial prototype synthesis were characterized by their physiochemical properties by DLS, FESEM, and UV−vis spectroscopy. These experiments confirmed the nanosize nature of TiO_2 nanoparticles as well as determined the surface charge modification with respect to a change in the size. Determination of the zeta potential and nanoparticle uptake in HCT116 cells illustrated the size- and charge-dependent interaction, followed by internalization of these nanoparticles. As demonstrated by the flow cytometry analysis and microscopy, TiO_2 nanoparticles were found to express the scavenging of ROS and eliciting the induction of LD cluster inside the cells. These results depicted the mechanism of cytotoxic effect of industrially prepared TiO_2 nanoparticles in the colon cell as a consequence of the ROS quenching and a probable role of lipid accumulation, leading to apoptosis and cell death. Cell cycle analysis revealed the arrest at the G_0/G_1 phase, suggesting the delay in DNA synthesis because of the TiO_2 nanoparticle exposure. In silico investigation revealed the crucial role of TiO_2 nanoparticle interactions with Sod, p53, and VLDLR proteins responsible for cytotoxicity. Additionally, synthesized TiO_2 nanoparticles

DOI: 10.1021/acsomega.7b01522
ACS Omega 2018, 3, 1244−1262

were exhibiting the antibacterial activity against *E. coli* and *S. typhimurium*. Live/dead flow cytometry assay described the size-dependent cell death of bacteria, however, the ROS analysis figured out the similar scavenging property by TiO_2 nanoparticles, as found in the case of mammalian cells. The zeta potential of the bacterial cells was also found to be altered with respect to the size and charge of the TiO_2 nanoparticles. The present study concludes that though TiO_2 nanoparticles are antibacterial, they are cytotoxic at higher concentrations and on prolonged exposure for mammalian cells. It also affects on the genomic level by influencing the DNA synthesis, which might be due to its nuclear deposition. Hence, it is imperative that their application in day-to-day life should be given special attention besides embracing the antibacterial potential.

■ ASSOCIATED CONTENT

Supporting Information

The Supporting Information is available free of charge on the ACS Publications website at DOI: 10.1021/acsomega.7b01522.

Change in the zeta potential and cell cycle arrest in HCT116 cells treated with different concentrations of HEBM synthesized TiO_2 nanoparticles (PDF)

■ AUTHOR INFORMATION

Corresponding Author

*E-mail: msbiotek@yahoo.com, msuar@kiitbiotech.ac.in (M.S.).

ORCID

Pritam Kumar Panda: 0000-0003-4879-2302

Arun Thirumurugan: 0000-0001-7261-988X

Mrutyunjay Suar: 0000-0002-2433-9100

Notes

The authors declare no competing financial interest.

■ REFERENCES

(1) Weir, A.; Westerhoff, P.; Fabricius, L.; Hristovski, K.; von Goetz, N. Titanium Dioxide Nanoparticles in Food and Personal Care Products. *Environ. Sci. Technol.* **2012**, *46*, 2242−2250.

(2) ICIS. *Titanium Dioxide (TiO_2) Uses and Market Data*.

(3) http://ec.europa.eu/environment/waste/titanium.htm. Titanium Dioxide.

(4) Van Bussel, W.; Kerkhof, F.; Van Kessel, T.; Lamers, H.; Nous, D.; Verdonk, H.; Verhoeven, B.; Boer, N.; Toonen, H. Accurate Determination of Titanium as Titanium Dioxide for Limited Sample Size Digestibility Studies of Feed and Food Matrices by Inductively Coupled Plasma Optical Emission Spectrometry with Real-Time Simultaneous Internal Standardization. *At. Spectrosc.* **2010**, *31*, 81−88.

(5) Mahata, S.; Mahato, S. S.; Nandi, M. M.; Mondal, B. Synthesis of TiO2 Nanoparticles by Hydrolysis and Peptization of Titanium Isopropoxide Solution. *Funct. Mater.* **2012**, *1461*, 225−228.

(6) Zhou, X.; Ni, S.; Zhang, X.; Wang, X.; Hu, X.; Zhou, Y. Controlling Shape and Size of TiO2 Nanoparticles with Sodium Acetate. *Curr. Nanosci.* **2008**, *4*, 397−401.

(7) Indris, S.; Amade, R.; Heitjans, P.; Finger, M.; Haeger, A.; Hesse, D.; Grünert, W.; Börger, A.; Becker, K. D. Preparation by High-Energy Milling, Characterization, and Catalytic Properties of Nanocrystalline TiO2. *J. Phys. Chem. B* **2005**, *109*, 23274−23278.

(8) Jesline, A.; John, N. P.; Narayanan, P. M.; Vani, C.; Murugan, S. Antimicrobial Activity of Zinc and Titanium Dioxide Nanoparticles against Biofilm-Producing Methicillin-Resistant Staphylococcus Aureus. *Appl. Nanosci.* **2015**, *5*, 157−162.

(9) Rompelberg, C.; Heringa, M. B.; van Donkersgoed, G.; Drijvers, J.; Roos, A.; Westenbrink, S.; Peters, R.; van Bemmel, G.; Brand, W.; Oomen, A. G. Oral Intake of Added Titanium Dioxide and Its Nanofraction from Food Products, Food Supplements and Toothpaste by the Dutch Population. *Nanotoxicology* **2016**, *10*, 1404−1414.

(10) Sohaebuddin, S. K.; Thevenot, P. T.; Baker, D.; Eaton, J. W.; Tang, L. Nanomaterial Cytotoxicity Is Composition, Size, and Cell Type Dependent. *Part. Fibre Toxicol.* **2010**, *7*, 22.

(11) Tedja, R.; Lim, M.; Amal, R.; Marquis, C. Effects of Serum Adsorption on Cellular Uptake Profile and Consequent Impact of Titanium Dioxide Nanoparticles on Human Lung Cell Lines. *ACS Nano* **2012**, *6*, 4083−4093.

(12) Thevenot, P.; Cho, J.; Wavhal, D.; Timmons, R. B.; Tang, L. Surface Chemistry Influences Cancer Killing Effect of TiO2 Nanoparticles. *Nanomed. Nanotechnol. Biol. Med.* **2008**, *4*, 226−236.

(13) Krüger, K.; Cossais, F.; Neve, H.; Klempt, M. Titanium Dioxide Nanoparticles Activate IL8-Related Inflammatory Pathways in Human Colonic Epithelial Caco-2 Cells. *J. Nanoparticle Res.* **2014**, *16*, 2402.

(14) Ahmed, D.; Eide, P. W.; Eilertsen, I. A.; Danielsen, S. A.; Eknæs, M.; Hektoen, M.; Lind, G. E.; Lothe, R. A. Epigenetic and Genetic Features of 24 Colon Cancer Cell Lines. *Oncogenesis* **2013**, *2*, No. e71.

(15) Nel, A. Toxic Potential of Materials. *Science* **2007**, *311*, 622−627.

(16) Saha, K.; Kim, S. T.; Yan, B.; Miranda, O. R.; Alfonso, F. S.; Shlosman, D.; Rotello, V. M. Surface Functionality of Nanoparticles Determines Cellular Uptake Mechanisms in Mammalian Cells. *Small* **2013**, *9*, 300−305.

(17) Li, Y.; Zhang, W.; Niu, J.; Chen, Y. Mechanism of Photogenerated Reactive Oxygen Species and Correlation with the Antibacterial Properties of Engineered Metal-Oxide Nanoparticles. *ACS Nano* **2012**, *6*, 5164−5173.

(18) Hackenberg, S.; Friehs, G.; Kessler, M.; Froelich, K.; Ginzkey, C.; Koehler, C.; Scherzed, A.; Burghartz, M.; Kleinsasser, N. Nanosized Titanium Dioxide Particles Do Not Induce DNA Damage in Human Peripheral Blood Lymphocytes. *J. Nanoparticle Res.* **2011**, *52*, 264−268.

(19) Gurr, J.-R.; Wang, A. S. S.; Chen, C.-H.; Jan, K.-Y. Ultrafine Titanium Dioxide Particles in the Absence of Photoactivation Can Induce Oxidative Damage to Human Bronchial Epithelial Cells. *Toxicology* **2005**, *213*, 66−73.

(20) Long, T. C.; Saleh, N.; Tilton, R. D.; Lowry, G. V.; Veronesi, B. Titanium Dioxide (P25) Produces Reactive Oxygen Species in Immortalized Brain Microglia (BV2): Implications for Nanoparticle Neurotoxicity. *Environ. Sci. Technol.* **2006**, *40*, 4346−4352.

(21) Ghosh, M. Cytotoxic, Genotoxic and the Hemolytic Effect of Titanium Dioxide (TiO2) Nanoparticles on Human Erythrocyte and Lymphocyte Cells in Vitro. *J. Appl. Toxicol.* **2013**, *33*, 1097.

(22) Zaki, S. S. O.; Ibrahim, M. N.; Katas, H. Particle Size Affects Concentration-Dependent Cytotoxicity of Chitosan Nanoparticles towards Mouse Hematopoietic Stem Cells. *J. Nanotechnol.* **2015**, *2015*, 1.

(23) Guichard, Y.; Schmit, J.; Darne, C.; Gaté, L.; Goutet, M.; Rousset, D.; Rastoix, O.; Wrobel, R.; Witschger, O.; Martin, A.; et al. Cytotoxicity and Genotoxicity of Nanosized and Microsized Titanium Dioxide and Iron Oxide Particles in Syrian Hamster Embryo Cells. *Ann. Occup. Hyg.* **2012**, *56*, 631−644.

(24) Arakha, M.; Pal, S.; Samantarrai, D.; Panigrahi, T. K.; Mallick, B. C.; Pramanik, K.; Mallick, B.; Jha, S. Antimicrobial Activity of Iron Oxide Nanoparticle upon Modulation of Nanoparticle-Bacteria Interface. *Sci. Rep.* **2015**, *5*, 14813.

(25) Chen, S.; Guo, Y.; Chen, S.; Ge, Z.; Yang, H.; Tang, J. Fabrication of Cu/TiO2 Nanocomposite: Toward an Enhanced Antibacterial Performance in the Absence of Light. *Mater. Lett.* **2012**, *83*, 154−157.

(26) Kubacka, A.; Diez, M. S.; Rojo, D.; Bargiela, R.; Ciordia, S.; Zapico, I.; Albar, J. P.; Barbas, C.; Martins dos Santos, V. a. P.; Fernández-García, M.; et al. Understanding the Antimicrobial Mechanism of TiO2-Based Nanocomposite Films in a Pathogenic Bacterium. *Sci. Rep.* **2014**, *4*, 4134.

(27) Zucker, R. M.; Massaro, E. J.; Sanders, K. M.; Degn, L. L.; Boyes, W. K. Detection of TiO2 Nanoparticles in Cells by Flow Cytometry. *Cytometry, Part A* **2010**, *77*, 677−685.

DOI: 10.1021/acsomega.7b01522
ACS Omega 2018, 3, 1244−1262

(28) Jung, W. K.; Koo, H. C.; Kim, K. W.; Shin, S.; Kim, S. H.; Park, Y. H. Antibacterial Activity and Mechanism of Action of the Silver Ion in Staphylococcus Aureus and Escherichia Coli. *Appl. Environ. Microbiol.* **2008**, *74*, 2171−2178.
(29) Nioi, P.; Perry, B. K.; Wang, E.-J.; Gu, Y.-Z.; Snyder, R. D. In Vitro Detection of Drug-Induced Phospholipidosis Using Gene Expression and Fluorescent Phospholipid-Based Methodologies. *Toxicol. Sci.* **2007**, *99*, 162−173.
(30) Kasibhatla, S. Acridine Orange/Ethidium Bromide (AO/EB) Staining to Detect Apoptosis. *Cold Spring Harb. Protoc.* **2006**, *2006*, pdb.prot4493.
(31) Trott, O.; Olson, A. J. AutoDock Vina: Improving the Speed and Accuracy of Docking with a New Scoring Function, Efficient Optimization and Multithreading. *J. Comput. Chem.* **2010**, *31*, 455−461.
(32) Pettersen, E. F.; Goddard, T. D.; Huang, C. C.; Couch, G. S.; Greenblatt, D. M.; Meng, E. C.; Ferrin, T. E. UCSF Chimera—A Visualization System for Exploratory Research and Analysis. *J. Comput. Chem.* **2004**, *25*, 1605−1612.
(33) Wallace, A. C.; Laskowski, R. A.; Thornton, J. M. Ligplot—a Program To Generate Schematic Diagrams of Protein Ligand Interactions. *Protein Eng.* **1995**, *8*, 127−134.
(34) Cao, W. Synthesis of Nanomaterials by High Energy Ball Milling. http://www.understandingnano.com/nanomaterial-synthesis-ball-milling.html.
(35) Sopicka-Lizer, M. *High-Energy Ball Milling*; Woodhead Publishing, 2010.
(36) Dharma, J.; Pisal, A.; Shelton, C. Simple Method of Measuring the Band Gap Energy Value of TiO2 in the Powder Form Using a UV/Vis/NIR Spectrometer. *Appl. Note* **2009**, 3−6.
(37) Zhang, Y.; Yang, M.; Park, J.-H.; Singelyn, J.; Ma, H.; Sailor, M. J.; Ruoslahti, E.; Ozkan, M.; Ozkan, C. A Surface-Charge Study on Cellular-Uptake Behavior of F3-Peptide-Conjugated Iron Oxide Nanoparticles. *Small* **2009**, *5*, 1990−1996.
(38) Tobergte, D. R.; Curtis, S. Synthesis of Nanomaterials by High Energy Ball Milling. http://www.understandingnano.com/nanomaterial-synthesis-ball-milling.html.
(39) Anuradha, T. V.; Ranganathan, S. Nanocrystalline TiO2 by Three Different Synthetic Approaches: A Comparison. *Bull. Mater. Sci.* **2007**, *30*, 263−269.
(40) Johnston, H. J.; Hutchison, G. R.; Christensen, F. M.; Peters, S.; Hankin, S.; Stone, V. Identification of the Mechanisms That Drive the Toxicity of TiO(2)Particulates: The Contribution of Physicochemical Characteristics. *Part. Fibre Toxicol.* **2009**, *6*, 33.
(41) Xu, R.; Wu, C.; Xu, H. Particle Size and Zeta Potential of Carbon Black in Liquid Media. *Carbon* **2007**, *45*, 2806−2809.
(42) Vasconcellos, S. R.; Kosman, J. J.; Rowell, R. L.; Medalia, A. I. The Relationship Between Zeta Potential and Particle Size in Non-Aqueous Carbon-Black Dispersions. *J. Dispersion Sci. Technol.* **1983**, *4*, 409−413.
(43) Prasad, R. Y.; Wallace, K.; Daniel, K. M.; Tennant, A. H.; Zucker, R. M.; Strickland, J.; Dreher, K.; Kligerman, A. D.; Blackman, C. F.; Demarini, D. M. Effect of Treatment Media on the Agglomeration of Titanium Dioxide Nanoparticles: Impact on Genotoxicity, Cellular Interaction, and Cell Cycle. *ACS Nano* **2013**, *7*, 1929−1942.
(44) Liao, D. L.; Wu, G. S.; Liao, B. Q. Zeta Potential of Shape-Controlled TiO2 Nanoparticles with Surfactants. *Colloids Surf., A* **2009**, *348*, 270−275.
(45) Berg, J. M.; Romoser, A.; Banerjee, N.; Zebda, R.; Sayes, C. M. The Relationship between pH and Zeta Potential of ∼30 Nm Metal Oxide Nanoparticle Suspensions Relevant to in Vitro Toxicological Evaluations. *Nanotoxicology* **2009**, *3*, 276−283.
(46) Fröhlich, E. The Role of Surface Charge in Cellular Uptake and Cytotoxicity of Medical Nanoparticles. *Int. J. Nanomed.* **2012**, *7*, 5577−5591.
(47) Verma, S. K.; Jha, E.; Panda, P. K.; Das, J. K.; Thirumurugan, A.; Suar, M.; Parashar, S. Molecular Aspects of Core-Shell Intrinsic Defect Induced Enhanced Antibacterial Activity of ZnO Nanocrystals. *Nanomedicine* **2018**, *13*, 43.
(48) Verma, S. K.; Panda, P. K.; Jha, E.; Suar, M.; Parashar, S. K. S. Altered Physiochemical Properties in Industrially Synthesized ZnO Nanoparticles Regulate Oxidative Stress; Induce in Vivo Cytotoxicity in Embryonic Zebrafish by Apoptosis. *Sci. Rep.* **2017**, *7*, 13909.
(49) Damonte, L. C.; Zélis, L. A. M.; Soucase, B. M.; Fenollosa, M. A. H. Nanoparticles of ZnO Obtained by Mechanical Milling. *Powder Technol.* **2004**, *148*, 15−19.
(50) Mishra, Y. K.; Adelung, R. ZnO Tetrapod Materials for Functional Applications. *Mater. Today* **2017**, DOI: 10.1016/j.mattod.2017.11.003. , In Press
(51) Duggal, N.; Jaishankar, D.; Yadavalli, T.; Hadigal, S.; Mishra, Y. K.; Adelung, R.; Shukla, D. Zinc Oxide Tetrapods Inhibit Herpes Simplex Virus Infection of Cultured Corneas. *Mol. Vision* **2017**, *23*, 26−38.
(52) Park, J. H.; Oh, N. Endocytosis and Exocytosis of Nanoparticles in Mammalian Cells. *Int. J. Nanomed.* **2014**, *9*, 51−63.
(53) Zhang, Y.; Yang, M.; Portney, N. G.; Cui, D.; Budak, G.; Ozbay, E.; Ozkan, M.; Ozkan, C. S. Zeta Potential: A Surface Electrical Characteristic to Probe the Interaction of Nanoparticles with Normal and Cancer Human Breast Epithelial Cells. *Biomed. Microdevices* **2008**, *10*, 321−328.
(54) Shapiro, H. M. Optical Measurements in Cytometry: Light Scattering, Extinction, Absorption, and Fluorescence. *Methods Cell Biol.* **2001**, *63*, 107−129.
(55) Kim, J. A.; Åberg, C.; Salvati, A.; Dawson, K. A. Role of Cell Cycle on the Cellular Uptake and Dilution of Nanoparticles in a Cell Population. *Nat. Nanotechnol.* **2011**, *7*, 62−68.
(56) Suzuki, H.; Toyooka, T.; Ibuki, Y. Simple and Easy Method to Evaluate Uptake Potential of Nanoparticles in Mammalian Cells Using a Flow Cytometric Light Scatter Analysis. *Environ. Sci. Technol.* **2007**, *41*, 3018−3024.
(57) Vranic, S.; Boggetto, N.; Contremoulins, V.; Mornet, S.; Reinhardt, N.; Marano, F.; Baeza-Squiban, A.; Boland, S. Deciphering the Mechanisms of Cellular Uptake of Engineered Nanoparticles by Accurate Evaluation of Internalization Using Imaging Flow Cytometry. *Part. Fibre Toxicol.* **2013**, *10*, 2.
(58) Fenoglio, I.; et al. Singlet Oxygen Plays a Key Role in the Toxicity and DNA Damage Caused by Nanometric TiO2 in Human Keratinocytes. *Nanoscale* **2013**, *5*, 6567.
(59) Cooper, G. M. *The Cell: A Molecular Approach*, 2nd ed.; Sinauer Associates, 2000.
(60) Antoine, T. E.; Hadigal, S. R.; Yakoub, A. M.; Mishra, Y. K.; Bhattacharya, P.; Haddad, C.; Valyi-Nagy, T.; Adelung, R.; Prabhakar, B. S.; Shukla, D. Intravaginal Zinc Oxide Tetrapod Nanoparticles as Novel Immunoprotective Agents against Genital Herpes. *J. Immunol.* **2016**, *196*, 4566−4575.
(61) Wang, Y.; Yao, C.; Li, C.; Ding, L.; Liu, J.; Dong, P.; Fang, H.; Lei, Z.; Shi, G.; Wu, M. Excess Titanium Dioxide Nanoparticles on the Cell Surface Induce Cytotoxicity by Hindering Ion Exchange and Disrupting Exocytosis Processes. *Nanoscale* **2015**, *7*, 13105−13115.
(62) Falck, G. C. M.; Lindberg, H. K.; Suhonen, S.; Vippola, M.; Vanhala, E.; Catalán, J.; Savolainen, K.; Norppa, H. Genotoxic Effects of Nanosized and Fine TiO2. *Hum. Exp. Toxicol.* **2009**, *28*, 339−352.
(63) Kang, S. J.; Kim, B. M.; Lee, Y. J.; Chung, H. W. Titanium Dioxide Nanoparticles Trigger p53-Mediated Damage Response in Peripheral Blood Lymphocytes. *Cell* **2008**, *49*, 399−405.
(64) Dubey, A.; Goswami, M.; Yadav, K.; Chaudhary, D. Oxidative Stress and Nano-Toxicity Induced by TiO2 and ZnO on WAG Cell Line. *PLoS One* **2015**, *10*, No. e0127493.
(65) Bhattacharya, K.; Davoren, M.; Boertz, J.; Schins, R. P. F.; Hoffmann, E.; Dopp, E. Titanium Dioxide Nanoparticles Induce Oxidative Stress and DNA-Adduct Formation but Not DNA-Breakage in Human Lung Cells. *Part. Fibre Toxicol.* **2009**, *6*, 17.
(66) Wang, J.; Fan, Y. Lung Injury Induced by TiO2 Nanoparticles Depends on Their Structural Features: Size, Shape, Crystal Phases, and Surface Coating. *Int. J. Mol. Sci.* **2014**, *15*, 22258−22278.
(67) Jelinek, R. *Science*; Walter de Gruyter GmbH & Co KG., 2015.

DOI: 10.1021/acsomega.7b01522
ACS Omega 2018, 3, 1244−1262

(68) Yadav, T. P.; Yadav, R. M.; Singh, D. P. Mechanical Milling: A Top Down Approach for the Synthesis of Nanomaterials and Nanocomposites. *Nanosci. Nanotechnol.* **2012**, *2*, 22−48.
(69) Vankoningsloo, S.; Piens, M.; Lecocq, C.; Gilson, A.; De Pauw, A.; Renard, P.; Demazy, C.; Houbion, A.; Raes, M.; Arnould, T. Mitochondrial Dysfunction Induces Triglyceride Accumulation in 3T3-L1 Cells: Role of Fatty Acid Beta-Oxidation and Glucose. *J. Lipid Res.* **2005**, *46*, 1133−1149.
(70) Semenza, G. L. Oxygen-Dependent Regulation of Mitochondrial Respiration by Hypoxia-Inducible Factor 1. *Biochem. J.* **2007**, *405*, 1−9.
(71) Przybytkowski, E.; Behrendt, M.; Dubois, D.; Maysinger, D. Nanoparticles Can Induce Changes in the Intracellular Metabolism of Lipids without Compromising Cellular Viability. *FEBS J.* **2009**, *276*, 6204−6217.
(72) Martin, S.; Parton, R. G. Lipid Droplets: A Unified View of a Dynamic Organelle. *Nat. Rev. Mol. Cell Biol.* **2006**, *7*, 373−378.
(73) Saquib, Q.; Al-Khedhairy, A. A.; Siddiqui, M. A.; Abou-Tarboush, F. M.; Azam, A.; Musarrat, J. Titanium Dioxide Nanoparticles Induced Cytotoxicity, Oxidative Stress and DNA Damage in Human Amnion Epithelial (WISH) Cells. *Toxicol. In Vitro* **2012**, *26*, 351−361.
(74) Ishikawa, K.; Ishii, H.; Saito, T. DNA Damage-Dependent Cell Cycle Checkpoints and Genomic Stability. *DNA Cell Biol.* **2006**, *25*, 406−411.
(75) Benchimol, S. p53-Dependent Pathways of Apoptosis. *Cell Death Differ.* **2001**, *8*, 1049−1051.
(76) Landsiedel, R.; Ma-Hock, L.; Van Ravenzwaay, B.; Schulz, M.; Wiench, K.; Champ, S.; Schulte, S.; Wohlleben, W.; Oesch, F. Gene Toxicity Studies on Titanium Dioxide and Zinc Oxide Nanomaterials Used for UV-Protection in Cosmetic Formulations. *Nanotoxicology* **2010**, *4*, 364−381.
(77) El Badawy, A. M.; Silva, R. G.; Morris, B.; Scheckel, K. G.; Suidan, M. T.; Tolaymat, T. M. Surface Charge-Dependent Toxicity of Silver Nanoparticles. *Environ. Sci. Technol.* **2011**, *45*, 283−287.
(78) Chen, S.; Guo, Y.; Chen, S.; Yu, H.; Ge, Z.; Zhang, X.; Zhang, P.; Tang, J. Facile Preparation and Synergistic Antibacterial Effect of Three-Component Cu/TiO2/CS Nanoparticles. *J. Mater. Chem.* **2012**, *22*, 9092−9099.
(79) Chen, S.; Guo, Y.; Zhong, H.; Chen, S.; Li, J.; Ge, Z.; Tang, J. Synergistic Antibacterial Mechanism and Coating Application of Copper/titanium Dioxide Nanoparticles. *Chem. Eng. J.* **2014**, *256*, 238−246.
(80) Su, H.-L.; Chou, C.-C.; Hung, D.-J.; Lin, S.-H.; Pao, I.-C.; Lin, J.-H.; Huang, F.-L.; Dong, R.-X.; Lin, J.-J. The Disruption of Bacterial Membrane Integrity through ROS Generation Induced by Nanohybrids of Silver and Clay. *Biomaterials* **2009**, *30*, 5979−5987.
(81) Brayner, R.; Ferrari-Iliou, R.; Brivois, N.; Djediat, S.; Benedetti, M. F.; Fiévet, F. Toxicological Impact Studies Based on Escherichi Coli Bacteria in Ultrafine ZnO Nanoparticles Colloidal Medium. *Nano Lett.* **2006**, *6*, 866−870.
(82) Kumar, A.; Pandey, A. K.; Singh, S. S.; Shanker, R.; Dhawan, A. Engineered ZnO and TiO(2) Nanoparticles Induce Oxidative Stress and DNA Damage Leading to Reduced Viability of Escherichia Coli. *Free Radical Biol. Med.* **2011**, *51*, 1872−1881.

DOI: 10.1021/acsomega.7b01522
ACS Omega 2018, 3, 1244−1262